CHALMERS

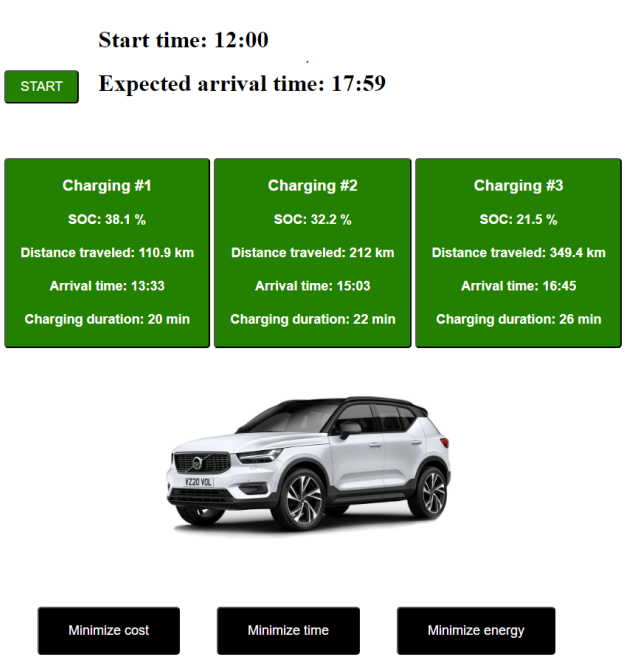

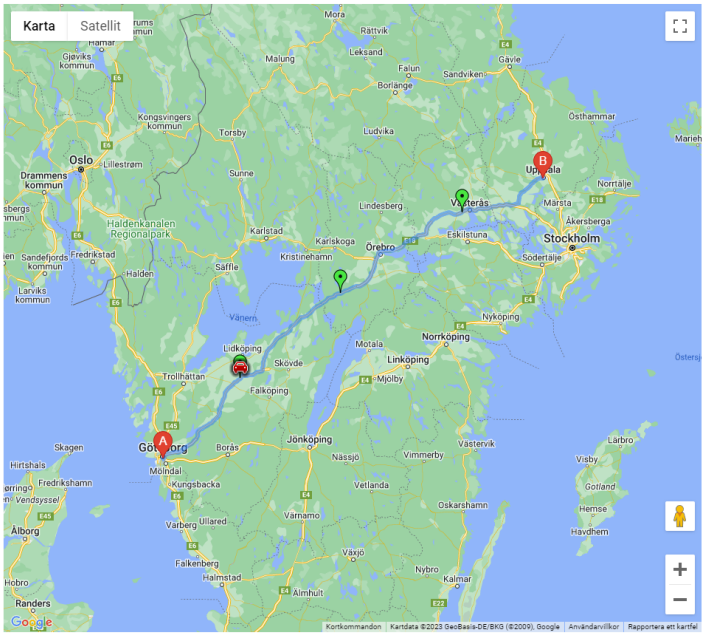

Intelligent trip-planning system for electric vehicles

Bachelor thesis

Henrik Bertilson, Hampus Burenius, Vincent Hellner, Victor Rodin, Jakob Svensson, Albert Ådén

DEPARTMENT OF ELECTRICAL ENGINEERING

CHALMERS UNIVERSITY OF TECHNOLOGY
Gothenburg, Sweden 2023
www.chalmers.se

Bachelor's thesis 2023

Intelligent trip-planning system for electric vehicles

Henrik Bertilson
Hampus Burenius
Vincent Hellner
Victor Rodin
Jakob Svensson
Albert Ådén

CHALMERS

Department of electrical engineering
Division of system and control
EENX16-23-25
Chalmers University of Technology
Gothenburg, Sweden 2023

Intelligent trip-planning system for electric vehicles
Henrik Bertilson
Hampus Burenius
Vincent Hellner
Victor Rodin
Jakob Svensson
Albert Ådén

Supervisor: Nikolce Murgovski, Division of Systems and Control
Examiner: Karinne Ramirez-Amaro, Division of Systems and Control

Bachelor's thesis 2023
Department Of Electrical Engineering
Division Of System and Control
EENX16-23-25
Chalmers University of Technology
SE-412 96 Gothenburg
Telephone +46 31 772 1000

Typeset in LaTeX
Printed by Chalmers Reproservice
Gothenburg, Sweden 2023

Abstract

This thesis describes the development of an intelligent trip planner for battery electric vehicles that account for battery temperature and charging station availability. The primary goal is to minimize cost, time, and energy consumption for drivers. The trip planner uses historical data to predict charging station availability and incorporates stochastic and mathematical models to optimize charging and battery temperature management. The project is a proof of concept for the construction of a route planner. Delimitations were applied to ensure project manageability, including data collection over a limited period, a predetermined driver profile, and three predefined routes for simulation.

The algorithm combines vehicle dynamics, availability distribution, and battery temperature management to calculate driving time and find the most optimal charging stations along the route. The predictive models for time to charge, energy consumption, and battery temperature estimation were verified through tests and compared with existing data. The optimization algorithm successfully found the best route from Gothenburg to Uppsala, and its results were verified by comparing them with existing route planners.

The study provides insights into the challenges and limitations of predicting energy loss during the charging process, highlighting the need for considering additional sources of energy loss in the model. Overall, the results demonstrate the potential for using optimization algorithms to enhance the efficiency and convenience of battery electric vehicles.

Acknowledgements

We would like to express our deepest gratitude to our supervisor Nikolce Murgovski for providing us with his time, encouragement, guidance, and invaluable support throughout the project. Nikolce's insightful suggestions have been instrumental in shaping the report and have greatly increased its quality. The group feels fortunate to have had the opportunity to work with such an incredible mentor.

The group would also like to give special thanks to Ahad Hamendia and Viktor Larsson from Volvo. For providing insight into vital components needed to construct the algorithm as well as providing the group with literature to evaluate the results of the thesis.

Lastly, we would like to acknowledge and give thanks for the great input we received from Petri Piiroinen in evaluating and constructing the vehicle dynamics model.

Henrik Bertilson, Hampus Burenius, Vincent Hellner, Victor Rodin, Jakob Svensson, Albert Ådén, Gothenburg, May 2023

List of Acronyms

Below is the list of acronyms that have been used throughout this thesis listed in alphabetical order:

AC	Alternating Current
API	Application Programming Interface
BEV	Battery Electrical Vehicle
DC	Direct Current
EOL	End Of Life
FWD	Front-wheel Drive
GCS	Geographic Coordinate System
GHG	Global Greenhouse Gases
ICE	Internal Combustion Engine
NVDB	Nationell Vägdatabas
PCM	Phase Change Material
REE	Rare Earth Elements
RUL	Remaining Useful Life
SoC	State of Charge
SoH	State Of Health
TTC	Time To Charge
UoC	Open Circuit Voltage
4WD	Four-Wheel Drive
ABRP	A Better RoutePlanner

Contents

List of Figures

List of Tables

1
Introduction

1.1 Background

This chapter provides background information regarding the environmental impact of the transport sector. Highlighting the need to reduce emissions from road passenger travel and introducing the EU's upcoming ban on the sale of new internal combustion engine (ICE) cars and small lorries. The discussion furthers to battery electric vehicles (BEV) and their emissions profile. The chapter then explores the customer and market demands on BEVs. It acknowledges the global growth in BEV sales while considering the challenges that remain. Finally, the chapter addresses the importance of trip time and charger availability, recognizing the impact of temperature on the BEV range.

1.1.1 Environmental background

In the last couple of years the global greenhouse gas (GHG) emissions have been around 50 billion tonnes of CO2 each year[1]. From the total emissions, the transport sector accounted for 16.2%, of which 60 % come from road passenger travel such as cars, motorcycles, and lorries. Decreasing the emissions from this sector could reduce global emissions by roughly 5 billion tonnes of CO2 yearly. The problem within the EU is similar with the transport sector increasing its emissions by 33% since the 1990 [2]. Due to this by the year 2035 a ban within the European union on sales of new ICE cars and small lorries will take effect [3]. When analyzing BEV it is important to not only study the emissions that occur when driving but also when manufacturing and at end of life (EOL). A major discussion point regarding BEVs is the large amount of energy and emittance produced in manufacturing. In countries with energy production with high intensity of GHG emissions as well as accounting for emissions in production and driving the BEV it on average reduces the total emissions by 25% when compared to an ICE vehicle, while in countries with lower GHG intensity such as Sweden, it accounts for a decrease of GHG by about 85% [4].

1.1.2 Customer and market demands on BEV

The adoption of BEVs could help reduce global emissions, but it will ultimately depend on consumers' willingness, accessibility to charging infrastructure, and cost. In 2020, there were 6.85 million BEVs worldwide, a 44% increase from the previous year [5]. However, this is still a relatively small percentage compared to the 66.7

million traditional vehicles sold in 2022 [6]. BEV sales vary by market, with Norway seeing the highest sales due to less concern about the cost and more concern about driving range, while in Germany and the US, the cost is a bigger concern [7]. The cost of BEVs is largely due to the powertrain, which includes the battery and accounts for 51% of the total cost [8]. The most common concerns about BEVs are limited range, higher costs, and lack of infrastructure for charging. However, as technology improves and costs decrease, BEVs are expected to become more accessible and desirable to consumers.

Sweden has set a target of a GHG neutral vehicle fleet by 2040 [9]. In order to reach this Sweden has also implemented several incentives such as subsidies and beneficial tax reduction legislation for owning a BEV [10]. Although the number of BEVs has increased in Sweden, the adoption rate is much slower than in neighboring countries [17]. Even though the financial benefits are the same all over Sweden there are also severe disparities between different municipalities in regards to BEV adoption rate. Based on the above the conclusion are that the main factors for low BEV adoption rate are due to high cost in comparison to ICE vehicle, geographical variation in accessibility to charging stations, increased trip time, and lack of sufficient incentives.

1.1.3 Importance of trip time and availability

As presented previously, the limited range is one of the main concerns when considering a transition to a BEV. Consequently, this limit leads to an increase in trip time due to more frequent charging. The trip time is dependent on the total capacity of the battery pack, the rate at which the battery is discharged, and the time spent charging. While the total capacity is reliant on the model of the vehicle and cannot be influenced much the discharge rate and time spent charging can both be minimized. According to C.Argue [12] extensively data analysis of over 5 million trips showed that the temperature of the climate has a significant impact on the range. Both cold and hot surrounding temperatures affect the range negatively. For a temperature of $-15°C$ the range drops on average as low as 54% of the range given by the manufacturers. As temperatures rise above $30°C$, the slope at which the range decreases increases, emphasizing that there is a range of optimal performance.

Another factor affecting the trip time is the availability of chargers. As stated in the customer and market demands, the accessibility to chargers plays a significant role in a customer's decision to switch to a BEV. In studies regarding the user experience of BEV users in Norway, it was found that range anxiety is transitioning to a charger anxiety[14][15]. This aligns whit what EY discovered in their recent mobility consumer study. Where lack of charging stations tops the list of the inhibitors of purchasing a BEV with 34% closely followed by range anxiety with 33% [16].

1.2 Purpose and goals

The purpose of the project was to develop an intelligent trip planner that takes into account battery temperature and is tasked with visualizing charging possibilities for

electric cars along the route from Chalmers University of Technology to Uppsala. This is to assist electric car users in finding a route that minimizes cost, time, and energy based on the driver's preferences.

The trip planner utilizes historical data on charging station availability along the selected route during the charging period. It employs stochastic models to plan and prioritize the choice of charging stations based on this historical data. Additionally, a mathematical model has been developed to compute energy consumption and regulate the battery's temperature.

The algorithm developed for the trip planner combines stochastic models and mathematical modeling to optimize the charging and temperature control based on given parameters. This provides electric car users with an efficient and reliable means of planning their trips, taking into account the battery temperature and available charging options along the route. The end result is a tool that assists electric car users in finding a route that minimizes cost, time, and energy consumption while also ensuring that the battery is properly charged and maintained.

The project works as a proof of concept for further examination of a route planner for BEV. The project especially focuses on battery temperature management in BEV, and availability prediction of electric chargers depending on time.

To specify the purpose, a clarification of the research question has been created, where the question has been divided into sub-goals that can be verified:

- Create a program that collects data on charger availability during the charging period along a specified route as a function of day and time of day.
- Specify stochastic models to plan and prioritize the choice of charging stations along the selected routes.
- Mathematically model the longitudinal dynamics of the vehicle to plan energy consumption and a thermal model of the battery to plan and regulate its temperature.
- Construct predictive models that accurately estimate charging time, battery temperature, and energy consumption during the charging process.
- Create an algorithm that combines the stochastic models and the mathematical modeling to then optimize the charging and temperature control based on given parameters.

1.3 Delimitations

To ensure the manageability of the project, delimitations regarding data collection, vehicle, driver, and route specifications, vehicle dynamics, battery health, and grid power were applied.

- **Data collection**: Due to limited possibilities to store information from charging stations, data collection will take place over a period of one month from

Chargefinder.com to then create a probability model based on charging trends. As it is built up from this historical data of charging stations, real-time updating will not be possible.

- **Vehicle, driver and route specifications**: The vehicle chosen for analysis was exclusively Volvo XC40 Recharge since it's one of the most sold BEVs currently in Sweden [10]. The driver profile will be predetermined and thus not be able to model different driving styles. The work is only a proof of concept, and the proposed method will be simulated on three predefined routes between Chalmers University and Uppsala University, in other words, the functionality will not be verified in a real vehicle.

- **Vehicle dynamics**: As for delimitations in relation to the dynamics of the vehicle, there was no modeling of the electrical motor, the torque was derived from mean acceleration with an upper limit of a maximum of 660 Nm. As well only the longitudinal dynamics will be accounted for, the lateral components will be disregarded. Also, all braking will be done by regenerative braking, this in order to limit the complexity of the model. Finally, no auxiliary loads such as fans, lights, heating, and cooling of the cabin compartment will be accounted for in the paper. This is due to its very limited effect on overall power consumption and battery temperature under the specified conditions.

- **Battery health**: Rather than providing a comprehensive analysis of battery health, the work will rely on estimations based on the state of charge and temperature. The reason for this is the belief that if performance boundaries are upheld, the lifespan of the battery will remain relatively unaffected. To elaborate, a state of charge interval between 20-80% was utilized, coupled with a temperature range of $0°C$ (based on the mean ambient temperature of the month of March for southern Sweden) to a maximum of $45°C$. In the event that the battery pack temperature approaches or surpasses the upper limits of this range, a battery thermal management system will be initialized.

- **Grid power**: In regards to the charging, the paper will not account for lower grid power induced by multiple cars charging at the same node. This is due to the complexity of both modeling this and obtaining the necessary information.

1.4 Social and ethical perspectives

Car batteries have an optimal lifespan when their operating range never exceeds 80% or falls below 20%. This results in less wear and tear on the battery and prevents significant capacity loss over time. Only during longer trips is it recommended to charge the battery to its maximum capacity. Charging according to this pattern can lead to poorer battery life and, in the worst case, early disposal of the battery. This is both economically and environmentally damaging because it requires vast amounts of resources, specifically rare earth elements (REE), to manufacture

batteries. REEs exist in the Earth's crust, but only in low concentrations. This means that their extraction is resource-intensive and often environmentally harmful. REEs used in batteries are a scarce resource globally and are produced using non-environmentally friendly methods [38].

A large part of the REEs used in battery production is found in countries that are more socioeconomically vulnerable to harsh and unhealthy working conditions. The current production of REEs is not only bad for the environment but also insufficient to meet existing demand. To address the problems with REEs, it is possible to produce new metals or recycle those that have already been used. Tesla, for example, recycles 92% of REEs from their batteries [39].

An important aspect of the work, therefore, is to weigh how driving should be determined between reducing time and cost for the driver, versus the more environmentally friendly choice of using less energy and not negatively affecting the battery's lifespan.

All data collected during the project has been focused on ensuring that the privacy of private and public citizens as well as companies is not negatively affected. The data collected is not sufficient to be able to identify any specific individuals and is only based on factors such as the cost, location, availability, and power of chargers at different times during the week and day. The data will also only be retained as long as needed to complete the project, afterwards, it will be discarded. Through the project, full transparency will be given as to how and where the collected data will be implemented.

1.5 Verification of goals

To ensure that the specified goals are accomplished they must be verified with suitable verification methods, hence the following methods have been established.

- The functionality of the data collection program will be verified by unit testing.
- To ensure the data collected is correct a logging sequence of the chargers will be run while their availability is manually checked on chargefinder.com. The logged data will then be compared to the manually collected data.
- To validate the accuracy of the stochastic models of availability they will be compared to real-time availability data.
- The mathematical model of the reliability of the longitudinal dynamic will be verified through simulations comparing the results to real-world data for the specified vehicle, with an acceptable error of 10%. While the thermal battery module will be verified by comparing the simulations to prior optimization work done by A.Hamendia [21].
- The verification of the predictive models for charging will involve the simulation of various scenarios and comparing them with each other and existing data to evaluate their accuracy.
- The effectiveness of the resulting algorithm will be verified through simulation. This will be done by evaluating its ability to optimize the preferred variable compared to an already existing trip planner.

2
Theory

The theory chapter consists of a brief description of the functionality of a BEV and the energy flow within the system. Additionally, the dynamics of a BEV are discussed explaining the factors affecting the energy consumption while driving. This is followed by information regarding the battery pack's structure and the charging/discharging physics. Furthermore, the chapter explains the thermal management of a battery pack and its vital applications. Following this is an overview of how chargers function. And lastly a concise explanation of a Markov chain.

2.1 Basic functionality of a BEV

BEV vehicles are fully electric, battery-driven, and rechargeable. The chemical energy within the battery is converted into electrical energy in the form of direct current (DC) and passed through an inverter that converts it into alternating current (AC) that in turn powers the engine. The Engine produces mechanical energy that is then transferred to a gearbox that in turn relays it to the wheels which propel the vehicle forward. The battery does not simply provide energy to the wheels but also auxiliary equipment. A lot of the steps of conversion within the BEV result in power losses and in turn limit the vehicle's performance. Below in Figure 2.1 is a simplified presentation of the energy flow within a BEV.

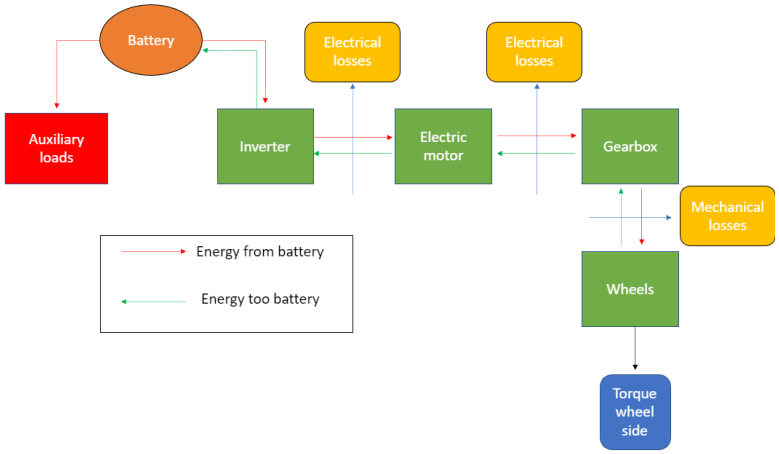

Figure 2.1: Schematic of energy flow within a BEV

- **Battery**: Converts chemical energy into electrical energy as DC, when discharging. And the other way around when in charging mode.

- **Inverter**: Receives DC power from the battery and converts it into AC. this process produces conversion losses.
- **Electric motor and Gearbox**: The motor receives AC power which is then connected to a gearbox, this process produces conversion losses. Unlike ICE vehicles which operate at a variety of different speeds and loads, generating the need for complex gearboxes with a lot of gear ratios, the electric motor has a flatter torque curve providing instant and consistent acceleration and speed control without the need for a traditional gearbox, resulting in a single-speed gearbox. [18].
- **Wheels**: From the gearbox to the wheels, the process works similarly to an ICE vehicle. Depending on the car's configuration, the energy is directed to the front, rear, or all wheels. The process produces mechanical losses.
- **Auxiliary loads**: The auxiliary loads are energy losses not directly connected to the propulsion of the vehicle. They range from large energy consumers such as air- conditioning, and heaters for battery and cabin compartments, to smaller such as pumps, fans, and lights.
- **Energy to the battery**: The energy generated by the battery flows in a similar way as energy from the battery. All regenerated energy is due to regenerative braking, more of this will be presented in succeeding chapters.

2.2 BEV Dynamics

The dynamics of a BEV are similar to an ICE vehicle since they both can be viewed as rigid bodies and the acting external forces are the same, but the generation of power and their transmission systems are different. An ICE vehicle's power is generated due to the ignition of fuel mixed with air while a BEVs power is provided by an electric motor driven by a consistent stream of electricity from its battery pack. The difference in the transmission systems is that a BEV due to its instant delivery of torque only needs one gear while an ICE vehicle needs an entire gearbox [29]. Another difference in the dynamics of the two vehicles is BEVs use of regenerative braking. During deceleration, the electric motor acts as a generator and converts part of the kinetic energy back to electric energy which is stored back in the battery pack [30]. The following sections will present relevant equations and knowledge to model the dynamics of a BEV.

2.2.1 Free body diagram of BEV

As mentioned earlier the vehicle can be viewed as a rigid body hence its external forces can be visualized in a free-body diagram, see Figure 2.2.

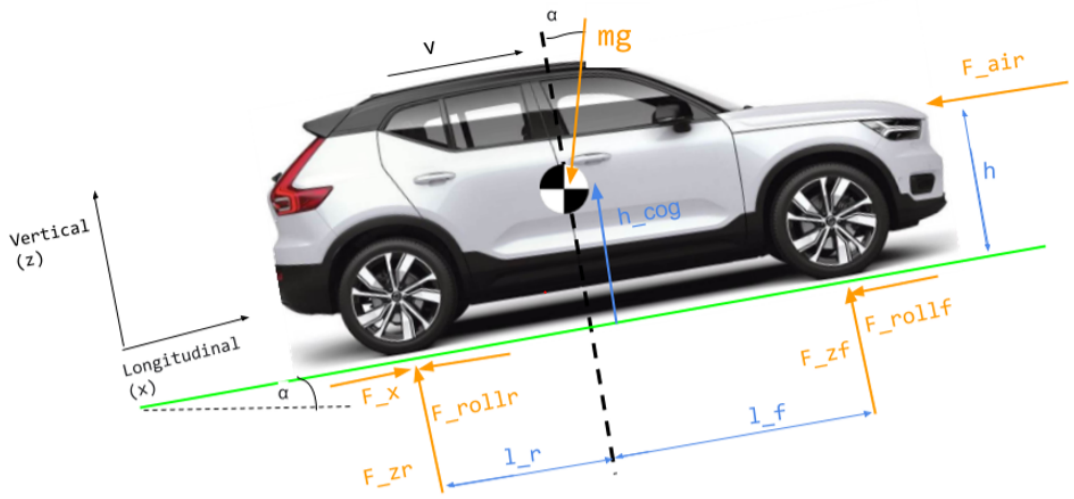

Figure 2.2: Free body diagram of the model Volvo XC40 Recharge

Seen in the free body diagram are the forces F_x, F_{rollr}, F_{rollf}, F_{zr}, F_{zf}, F_{air} and mg $[N]$ where r and f represent rear and front of the vehicle. F_x is the force due to traction delivered by the electrical motor. The force from rolling resistance between the road and the tire is denoted as F_{rollr} and F_{rollf}. F_{zr} and F_{zf} represent the reaction forces acting on the vehicle due to the force applied to the ground by its mass mg. Last the drag force denoted as F_{air}.

The force required by the motor is defined by the next equation. T $[N \cdot m]$ is the torque by the wheel, r $[m]$ is the radius of the wheel, $\eta_{inverter}, \eta_{motor}, \eta_{gearbox}$ are the efficiencies of the inverter, the motor, and the gearbox.

$$F_x = \frac{T}{r \cdot \eta_{inverter} \cdot \eta_{motor} \cdot \eta_{gearbox}} \tag{2.1}$$

To model only the longitudinal dynamics F_{rollr} and F_{rollf} can be combined into F_{roll}. The longitudinal components of F_{zr} and F_{zf} can be described as one variable using some simple trigonometry and the knowledge that gravity exists on Earth. $m_{vehicle}$ $[kg]$ is the total mass of the vehicle, g $[m/s^2]$ denotes earth's gravitational constant and α $[°]$ is the road gradient.

$$F_{roll} = F_{rollr} + F_{rollf} \tag{2.2}$$

$$F_{zrlong} + F_{zflong} = F_{gradient} = m_{vehicle} g(sin(\alpha)) \tag{2.3}$$

With the use of Newton's second law of motion that says that the sum of all forces on an object is equal to its acceleration $a_{resulting}$ $[m/s^2]$ times mass $m_{vehicle}$ $[kg]$, hence the resulting acceleration of the vehicle can be described accordingly.

$$F_{resulting} = m_{vehicle}a_{resulting} = F_x - F_{roll} - F_{gradient} - F_{air} \tag{2.4}$$

The resulting acceleration and the distance driven will determine the power consumed as the required torque from the motor is dependent on the acceleration; a greater acceleration will lead to higher drainage of the battery. The equation for carried out work by the motor over a distance can be seen below.

$$E_{consumed} = \int_{x_{start}}^{x_{end}} F_x(x) \quad dx \tag{2.5}$$

2.2.2 Resistive forces and energy recovery

The subsequent section is an explanation of the resistive forces which consume energy and the energy recuperated due to regenerative braking.

- **Rolling resistance force**:
  The force applied due to rolling resistance is caused by two factors, the deformation of the tyre's contact area with the ground and the damping properties of the rubber. This leads to an energy loss in the form of mechanical energy converting into heat [31]. The force can be determined using the following equation where C_r is the rolling resistance coefficient which varies due to the velocity of the vehicle, the material of the tyre, the material of the ground, and temperature [32].

$$F_{roll} = m_{vehicle}g(cos(\alpha))C_r \tag{2.6}$$

- **Drag force**:
  When an object moves through a fluid the object is subjected to a resistant force. This force is called drag force and acts in the opposite direction of the velocity of the object. It is caused due to the difference in velocity between the fluid and the object, it depends on the following factors, the density of the fluid ρ_{fluid} $[kg/m^3]$, an aerodynamic coefficient C_d, the frontal area of the object subject to drag A_{front} $[m^2]$ and the velocity of the object $v_{vehicle}$ $[m/s]$. [33]. For a BEV the fluid of interest is air, both the aerodynamic coefficient and frontal area vary depending on the model of the vehicle and the drag force can be computed with the following equation:

$$F_{air} = \frac{\rho_{fluid}C_dA_{front}v_{diff}^2}{2} \tag{2.7}$$

- **Regenerative braking**:
  Regenerative braking is a system that activates while braking in a BEV. The system is used to recover otherwise lost kinetic energy while braking. In an ICE vehicle while braking all kinetic energy of the vehicle is converted into heat and counts as a loss. As stated earlier a BEV uses an electrical motor to provide power to then drive the wheels and the vehicle forward, while braking or not accelerating the wheels will rotate the electric motor and hence work as a generator creating electricity used to recharge the battery [30]. The energy recovered is based on the force of the braking applied by the driver. A higher force will result in a larger energy recovery but there is an upper limit. For the Polestar 2 braking with a force of more than 0.3g will activate the regular mechanical brakes and the maximum recovered power is 100 kW [34]. The regenerated energy can be described using equation 2.8, this is derived from equation 2.4 while $F_{resulting} < 0$. η_{regen} refers to the efficiency of the regenerative braking system.

$$E_{recovered} = \int_{x_{start}}^{x_{end}} F_x(x) \cdot \eta_{regen} \quad dx \tag{2.8}$$

- **Tyre slip**:
  Tyre slip is a phenomenon in automotive vehicle dynamics that occur when the tyre's rotational velocity is either greater than or less than the velocity of the vehicle moving forward. The reason for a slip occurring is poor traction. The max traction force before slip occurs is dependent on the friction coefficient μ_{road} and the vertical force $F_{vertical}$ applied by the vehicle as seen in the following equation.

$$F_{tracmax} = \mu_{road} F_{vertical} \tag{2.9}$$

  Slip is often described as a percentage of the difference between the tyre's rotational velocity ω_{wheel} $[rad/s]$ and the vehicle's velocity using the following equation, where S_x is the slip rate [36]. With the use of the slip rate, an energy loss can be computed.

$$S_x = \frac{\omega_{wheel} r_{wheel} - v}{v} \tag{2.10}$$

2.3 EV battery pack

In BEVs the battery pack functions as the final and conclusive battery system [40]. The pack consists of an assembly of battery modules that are of a specific configuration depending on the vehicle's power requirements. They can be connected in parallel, in series, or both to meet these requirements. These modules, in turn, are constructed by battery cells that are assembled in a similar manner to the modules with a particular arrangement of series and parallel connections. The cells have three main forms cylindrical, prismatic, and pouch with the first mentioned being the most common. Ultimately, chemical energy is stored inside the battery cells, with the voltage of a single cell depending on the cell chemistry, which is primarily Lithium-ion at present. A visualization of a BEV battery pack and its components can be seen in Figure 2.3.

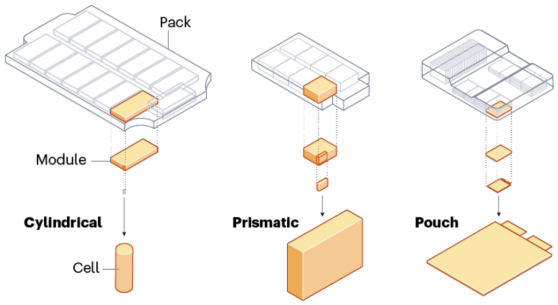

Figure 2.3: Eveenergi, *Electric battery management*, https://www.evenergi.com/electric-battery-management/

2.3.1 EV battery cell

A generic BEV lithium-ion battery consists of an anode, cathode, separator, and electrolyte. There are two electrical contact terminals, one positive and one negative with a potential difference of about 3-4 V, this is more commonly known as open circuit voltage (UoC)[19]. Discharging occurs when the vehicle is drawing energy from the battery and a chemical reaction occurs in the negative anode resulting in a flow of ions creating a current and converting chemical energy to electrical. When discharging, the state of charge (SoC), voltage, and chemical energy decrease. In order to increase the energy the process is reversed while charging, the flow ions are reverted and flow from a positive cathode to the negative anode increasing the SoC, voltage, and chemical energy. The UoC when charging and discharging is mainly affected by the difference in SoC, a visual representation can be seen below in Figure 2.4.

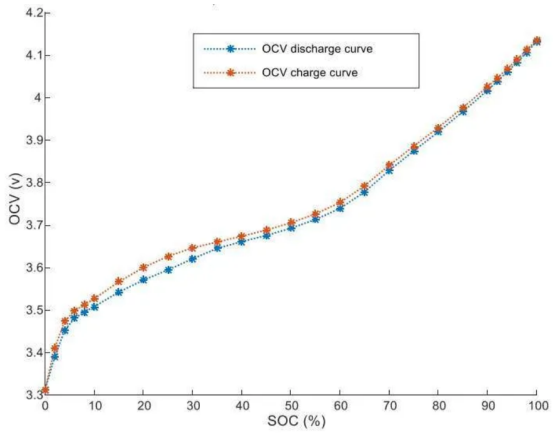

Figure 2.4: C. Zhang et al, *A Generalized SOC-OCV Model for Lithium-Ion Batteries and the SOC Estimation for LNMCO Battery* 2016

Charging and discharging (equation 2.11) incurs irreversible heat losses such as ohmic resistance losses as presented in equation (2.12). [21].

$$S\dot{o}C = \frac{P}{C_b U_{oc}} \tag{2.11}$$

$$Q^{gen}_{irreversibel}(t) = R_b(T_b)\frac{P^2(t)}{U^2_{oc}(SoC(t))} \tag{2.12}$$

The internal resistance $R_b(T_b)$ $[m\Omega]$ is dependent on temperature in such a way, that when the temperature of the battery increases the internal resistance lowers converging at about $25.166\,m\Omega$, making it easier for the ions within the battery to flow [22].

$$R_b(t) = 90.196e^{-0.08T_b(t)} + 25.166 \tag{2.13}$$

The temperature limits for attaining the best power discharging and charging is between $25°C - 45°C$ [21]. Resulting in that it's favorable to precondition the battery thermally before charging, to attain the highest power gain while minimizing irreversible losses.

2.3.2 State of health

A battery state of health (SoH) is a way of measuring the degradation and capacity of a battery. It is most commonly represented as a percentage of the original rated capacity of the battery. When the battery cell deteriorates it will experience a loss in power and an increase of the internal resistance. Maintaining a high state of health is therefore of utmost importance in order to keep the battery running at a good capacity for longer.

Remaining useful life (RUL) is another important measure according to Nuhic et al [23] referring to the number of discharge-charge cycles for the battery until EOL. When the RUL has reached 80% of the rated capacity of the battery it is considered EOL [24]. In order to extend the lifespan of a BEV battery the SoC when discharging and charging should be kept between 80% - 20% this will increase the number of discharge-charging cycles by roughly eight times, in comparison to fully charging and depleting the battery [25]. Temperature also plays a big part in the degradation of the battery. With no active current, a battery exposed to 20°C ambient temperature will degrade to 80% and EOL at roughly six years. Furthermore, if the ambient temperature were to increase to 35°C this degradation would take just about two years [26]. When you hit EOL the second life cycle kicks in[27], this means that the battery still has power left but the discharge-charge cycle is no longer optimal for a BEV. There are however a few uses left for the battery, some companies such as Nissan and Toyota use the retired batteries in other applications such as providing backup power for Amsterdam arena [27]. When the battery has degraded further and is no longer useable in alternative applications it is sent for recycling. Companies like Hydrovolt a subsidiary of Northvolt can recycle up to 95% of the battery mass and aims to have 50% of its production of new batteries produced by recycled materials by 2030 [28].

2.4 Thermal management of battery

As concluded earlier the battery of a BEV is one of the costliest components and one of the most important parts for optimal performance. Firstly the operating temperature of the battery affects its discharging and charging power. Equation (2.13) incentives that an increase in temperature results in lower internal resistance and vice versa with a decrease. This means that the battery power will deteriorate faster if not correctly conditioned, and it will charge slower if charged during suboptimal temperatures due to the affected flow of ions. With the correct usage of this knowledge, the trip time can be reduced significantly. Ahad, H concludes that if the battery temperature is kept at $25°C - 45°C$ the trip time could be reduced by as much as 44% [21]. The second important part of managing the temperature of the battery is its impact on SoH. As previously stated, a larger temperature will decrease the longevity of the battery which would result in the need for more frequent replacement of the battery. And to its high manufacturing cost, this is of uttermost importance to minimize. The final crucial aspect of the thermal management of lithium-ion cells is to prevent thermal runaway. This is a phenomenon in which

the cell reaches a temperature that triggers an unrestrained self-sustained heating state and ends with battery failure or fire [51]. Thermal runaway can be instigated by factors such as internal short circuits, overcharging or high temperatures [52]. In order to manage the temperature, a comprehensive understanding of how heat transfers within a battery pack and its surrounding are of relevance.

2.4.1 Heat transfer

Heat transfer refers to the exchange of thermal energy as heat amongst different objects [37]. At which rate this transfer happens is dependent on the temperature difference between the systems and what kind of medium through which the heat is transmitted. Heat can only travel from an object to an object with a lower temperature. There are three ground mechanisms of heat transfer, conduction, advection, and radiation. In engineering, it is more common to refer to advection as convection, which is a combination of conduction and advection. Seen below is a brief description of the three.

- **Conduction**: Diffusion of energy caused by random molecular movement, the energy movement can be described using this equation.

$$Q_{conduction} = -kA\frac{dT}{dx} \tag{2.14}$$

  k $[W/m*K]$ is the thermal conductivity which is the ability to transport heat of the material which the heat is transferred through. A $[m^2]$ refers to the area of the object subject to the transfer and $\frac{dT}{dx}$ is the temperature change over time.

- **Convection**: Conduction combined with energy transfer due to mass transport, calculated using the following equation. There are three types of convection that can occur, natural, forced, and a mix of both. The first mentioned results from the difference in density and gravitational forces. Forced is caused by a flow of a fluid.

$$Q_{convection} = h_{convection}A_s(T_s - T_{ambient}) \tag{2.15}$$

  A_s $[m^2]$ is the area of the surface exposed to the convective heat transfer, T_s $[°C]$ is the temperature of the surface and $T_{ambient}$ $[°C]$ indicates the temperature of the surrounding medium. $h_{convection}$ $[W/m^2*K]$ denotes the convection heat transfer coefficient and is calculated using the Nusselt number for the fluid flow causing the mass transport using the latter equation.

$$Nu = \frac{hL}{k_{fluid}} \tag{2.16}$$

  Nusselt number is a dimensionless number that denotes the ratio of convective to conductive heat transfer. Using its correlation with the Reynold and Prandtl number for the flow it can be evaluated with the general equation below.

$$Nu = aR_x^b Pr^c \tag{2.17}$$

Reynolds number is a dimensionless quantity that is used to decide whether a flow can be considered laminar or turbulent. It is based on the density of the fluid ρ_{fluid} $[kg/m^3]$, velocity of the fluid v_{fluid} $[m/s]$, length of the object prone to the flow L $[m]$ and lastly the dynamic viscosity of the fluid μ_{fluid} $[kg/m \cdot s]$.

$$Re = \frac{\rho_{fluid} v_{fluid} L}{\mu_{fluid}} \tag{2.18}$$

Prandtl number Pr is an experimental dimensionless parameter that provides a "measure of the relative effectiveness of momentum and energy transportation by diffusion in the velocity and thermal boundary layers" [37]. Its value can be obtained from experimental tables.

- **Radiation**: Energy transfer by electromagnetic waves. Radiation is generally only noticeable at higher temperatures than what is covered in this project.

2.4.2 Thermal management systems of battery pack

Air cooling, liquid cooling, and phase change material (PCM) cooling are three commonly used thermal management methods used in BEVs to cool the battery pack. Among these methods, air cooling is the least complex which only uses convection to dissipate the heat. This is achieved by creating an airflow around the battery modules using a fan that can either transport air from the cabin compartment or use ambient air [41]. The drawback of using air to cool the battery is that it has a lower convective heat transfer compared to other fluids. Additionally, the effectiveness of the heat transfer is also reliant on the temperature of the incoming air. See Figure 2.5 for an air-cooled system.

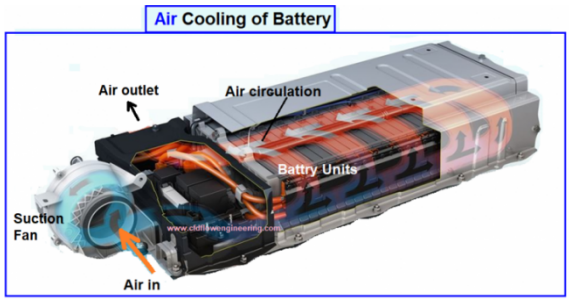

Figure 2.5: CFD Flow Engineering, *Battery Cooling Techniques in Electric Vehicle* https://cfdflowengineering.com/battery-cooling-techniques-in-electric-vehicle/#Liquid_cooling_of_Battery

Cooling with a liquid does not have these issues but it is a more expensive and complex solution. There are two main types of liquid cooling, direct and indirect cooling. Direct involves circulating the coolant with direct contact with either the battery cells or modules of the battery pack. In contrast, indirect cooling circulates

the liquid through tubes or cooling plates which are then in contact with the battery modules [42]. In Figure 2.6 an indirect liquid cooling system can be seen.

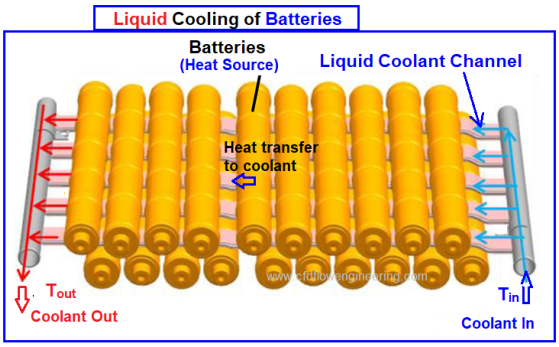

Figure 2.6: CFD Flow Engineering, *Battery Cooling Techniques in Electric Vehicle* https://cfdflowengineering.com/battery-cooling-techniques-in-electric-vehicle/#Liquid_cooling_of_Battery

The last method is based on the principle that a PCM transitioning from solid to liquid is an endothermic process and from liquid to solid is an exothermic process. Endothermic means that it absorbs heat from its surroundings and exothermic the opposite. The melting points of the materials utilized in this method are selectively adjusted to maintain the temperature within the desired range. In practice, such material is then placed in contact with the battery cells or modules. This is with the intent of dissipating heat when the battery pack's temperature increases beyond the acceptable range and transferring heat to the pack while operating below optimal temperatures [43]. See Figure 2.7 below for an example of a PCM system.

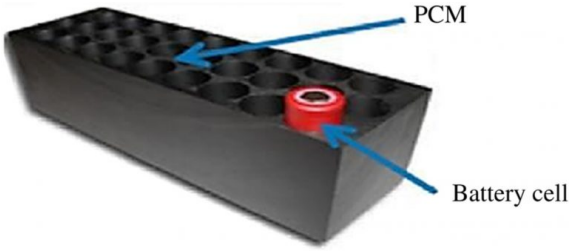

Figure 2.7: CFD Flow Engineering, *Battery Cooling Techniques in Electric Vehicle* https://cfdflowengineering.com/battery-cooling-techniques-in-electric-vehicle/#Liquid_cooling_of_Battery

2.5 Chargers

According to the European Commission, in the first quarter of 2023, there were roughly 3000 DC and 22 000 AC chargers that can be publicly accessed in Sweden [10]. The most common AC chargers generally operate on a capacity span of between 7 kW to 22 kW, but there are versions that can be less than 7 kW and above 22 kW. The chargers operate in such a way that it sends an AC current from the grid into the BEV inverter that then converts it to DC current so the battery

can store it, as visualized in Figure 2.8 below. Typically, these types of charges are slower and are commonly found at the homes of BEV users [44]. This is because the vehicle can gradually charge overnight or while it is parked.

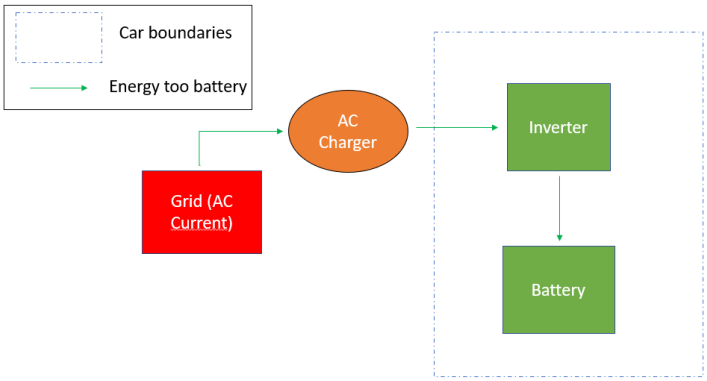

Figure 2.8: Visual representation of energy flow between grid and battery, AC charger.

In Sweden, the charging capacity of DC chargers can range from about 50 kW to 350 kW [10]. These chargers draw AC current from the grid and use a built-in rectifier to convert it to DC current for charging the BEV battery, see Figure 2.9 below. Compared to AC chargers, DC chargers are much faster and are usually located near major roads and gas stations. The speed at which a BEV can charge up to 80% battery and the amount of power it can utilize from an AC charger depends on various factors, including the charger's capacity, the current state of charge, and the grid demand induced by other BEV users charging. Typically, the time it takes to fully charge a normal-size BEV varies from 18 minutes for a 150 kW charger to 54 minutes for a 50 kW charger.

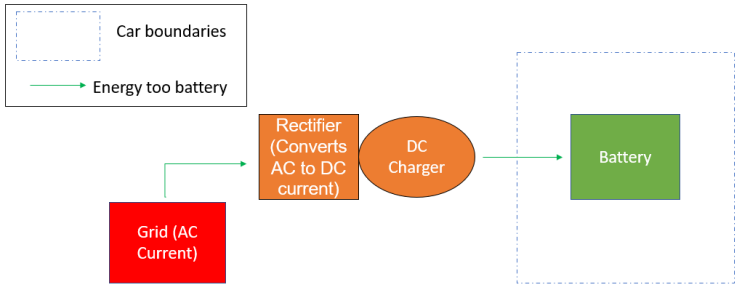

Figure 2.9: Visual representation of energy flow between grid and battery, DC charger.

The cost of charging at a publicly accessible charger depends on several factors. These include the charger's capacity and the current electricity price for the specific region of the power grid. This makes it challenging to compare refueling costs

between BEVs and ICE vehicles. However, it can be generally stated that as long as the electricity price remains below 6.5 kr/kWh, it is more cost-effective to charge and drive a BEV than an ICE vehicle [45].

2.6 Markov chain

A Markov chain is a stochastic model that represents a finite directed graph, with transition probabilities for each edge [53]. Stochastic models are models that depend on random variables. A Markov chain is a process for determining future events given the current state and a network of vertices and edges. The vertices represent the different states where the process can occur, and the edges are the possible transitions that each state can take. A visual representation of a Markov chain with 2 chargers and 3 states can be seen in Figure 2.10, where $p_m n$ represents the possible transitions and s_x represents each state. Each state in a Markov chain is only dependent on the previous state. The current state S_i can therefore only lead to one of a predefined set of states $S = [S_1, ..., S_n]$.

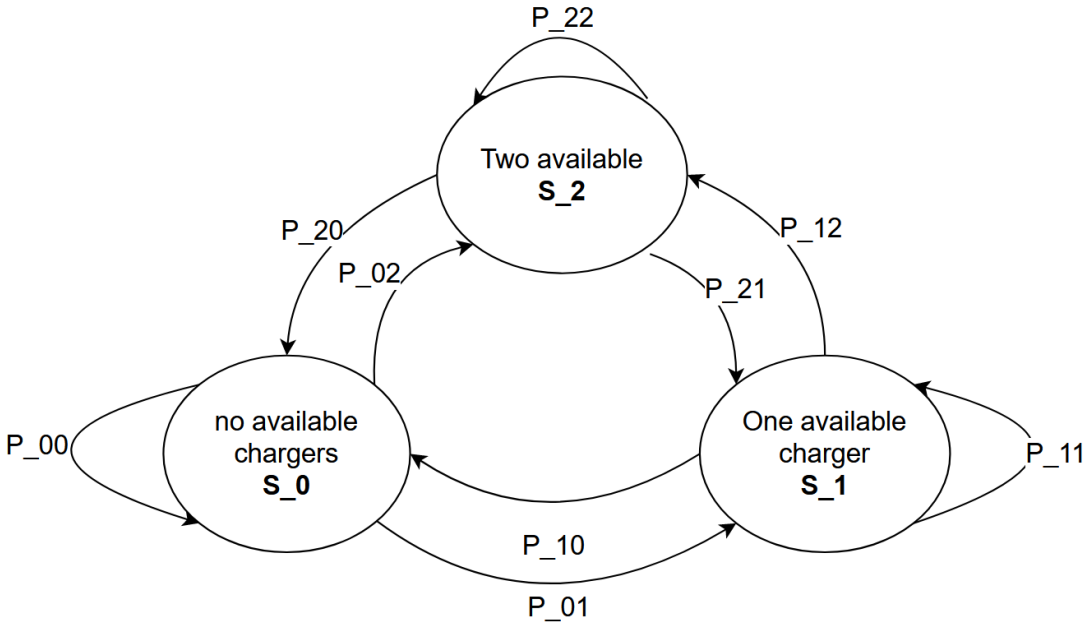

Figure 2.10: Visual representation of Markov chain transition states for a charging station containing two chargers of the same capacity. The number of available chargers is described by the state S_n with n being the number of free chargers.

Using Markov chain method, a model can be devised describing the current charging availability, where each state S_n represents the amount of available chargers at the charging station at a given time [54]. The predefined states of a station with n chargers would be $S = [0, 1, ...n - 1, n]$.

The model describes the possible states that each charging station can possibly achieve, and at which time. The state probabilities are calculated from a time-

dependent transition matrix, where each of the states $S_t = [S_{0,t}, S_{1,t}, ..., S_{0,t}]^T$ either transitions to another state or stay the same. The Transition matrix is of size $[n \cdot n]$ where n is the number of states.

$$T_t = \begin{bmatrix} p_{00,t} & p_{01,t} & \cdots & p_{0n,t} \\ p_{10,t} & p_{11,t} & \cdots & p_{1n,t} \\ \vdots & \vdots & \ddots & \vdots \\ p_{n0,t} & p_{n1,t} & \cdots & p_{nn,t} \end{bmatrix}$$

where

$$\sum_{j=1}^{n} p_{ij,t} = 1 \tag{2.19}$$

and

$$S_{t+dt} = S_t \cdot T(t + dt) \tag{2.20}$$

here $p_{ij,t}$ is the time independent transition probability to transition from state S_i to S_j. Equation (2.19) describes that the probability of all states is equal to 1. Equation (2.20) describes how the state at the next time point $t + dt$ is calculated as the product of the current state and the transition matrix. As an example, if the probability at a given moment t of the state changing from 1 available charger to zero being 50% then $p_1 0,_t = 0.5$. The state probabilities and transition matrix are calculated from collected data, where the availability and transitions for a specific time are the total gathered data at that time t.

3
Method

The method chapter encompasses a detailed description of all the steps taken during the development of the trip planner. It begins with a section depicting the process of data collection for the chargers on the given routes, the road data, and how the acquired data was structured. Furthermore, the next section explains the structure of the mathematical model of longitudinal vehicle dynamics. Additionally, it clarifies how stochastic models were used in order to predict charging time and availability. The final section describes how the trip planner algorithm integrates all the previous components to accomplish the objectives of this work.

3.1 Data collection and structuring

The following section provides an overview and description of the collection and structuring of the data collected for the charging stations, the road, and charging behavior.

3.1.1 Charging station data collection

Data from the charging stations were gathered from *chargefinder.com* via their API. It is structured so that general information such as name, location, and owner is found under *https://api.chargefinder.com/station* while status and availability are available via *https://api.chargefinder.com/status*.

Apart from this, the unique identifier for the specific charger in which availability data is wanted needs to be supplied. The identifier for each charger we wanted was gathered using Chrome DevTools by monitoring the traffic on *chargefinder.com* and seeing which API requests were made when selecting a charger.

A logging software was created which sends API requests for each charger once every 30 minutes and saves their availability status. This way a time series was created.

During the development of the logger, a number of problems arose. First and foremost Chargefinder would not accept simple API requests sent from Python as it seemed it only accepted requests sent from browsers. Specific headers had to be added to the requests in order for them to be valid and treated as if being sent from a browser. See appendix listing A.1 for these headers.

Another problem came up when grouping the chargers based on capacity. Not only was the number of chargers available at a given station wanted but specifically the amount of each capacity. In the */station* response chargers were divided into groups based on their characteristics (including capacity). But this information was not present in the */status* response. Instead, every charger on the */status* response had an "id" key.

The problem was that how this "id" corresponded to the chargers on the */station* response differs between stations. Some chargers have a "name" key while others have an "identifier" and some have both. This meant that it would be too computationally expensive to go through each possible mapping for every station we logged every time. Instead, this calculation had to be done before all the logging and cached. A dictionary that mapped the "id" of chargers on */status* to a number corresponding to their group on */station* was created. At first, there were problems with this as well since some "ids were the same between chargers on different stations. This was addressed by prefixing the key of the dictionary entries with the id of the actual station (see appendix listing A.2 for the code).

The structure of the dictionary file is then

```
<station_id><outlet_id> <outlet_list_index>
<station_id><outlet_id> <outlet_list_index>
<station_id><outlet_id> <outlet_list_index>
...
```

As some charger's availability status was unknown at the time of generating this dictionary and chargefinder therefore did not list them in the response there are some missing outlets from this dictionary that have to be ignored in the logging. The same is true if new outlets are added or changed at a station at a later date.

There were also some outlets that were listed twice with the same "id" on the same station. These chargers never differed in capacity, only in socket type. Our hypothesis is then that these were actually the same outlets just with multiple different sockets and therefore they are counted as one in the logging and only listed once in the dictionary.

The biggest problem which occurred when moving from logging a few chargers to logging all of them was that a limit on Chargefinder was reached. After logging a few times the logger crashed and the API response had a 403 status code which meant that the server had refused to authorize the request. This meant that chargefinder had started a cooldown on API requests. Unfortunately, this could only be solved by either logging less data or by making the logger wait after it had received the first 403 response. After examination, it was established that the cooldown was around 5 minutes which was determined to be small enough that waiting would be possible without negatively affecting the continuity of the time-series data too much. General error handling on the API requests was added which waits if a 403 error occurs and skips the entry if any other error comes up (see appendix listing A.3 for

the code).

Querying the database was done using a program separate from the logger. At first, a simple program was designed which simply asked which station or stations' availability data wanted to be queried and saved this to a JSON file. Later on, this turned out to be a good way of creating backups of the data by running this program on a schedule once every day and saving all of the data. The program was modified to allow this by adding timestamps to the resulting JSON filenames.

3.1.2 Road data collection

An initial and critical stage in the development of the trip planner involves the gathering and structuring of essential road data required for the simulation of vehicle dynamics during driving. In order to simulate the driving of a car, it was determined that data points representing changes in speed limits should be selected. Within these points, the car's acceleration or deceleration can be assumed based on the orientation of the preceding and subsequent speed limits. The resulting acceleration and energy consumption of the vehicle while moving from one data point to another can be calculated. More information on this process is provided in a subsequent chapter. Additionally, this understanding of driving dynamics enables the identification of the necessary data to collect from the road, including speed limits, distances between speed limit changes, and the gradient between speed limit changes.

3.1.2.1 Speed limit points

The data points where the speed limit changes were collected from Nationell Vägdatabas (NVDB)[48] which is Trafikverkets database over the road network in Sweden. One problem which occurred when gathering the points was that NVDB does not use the same geological reference system as was needed to gather data on the elevation and road distances from Google's API, namely the Geographic Coordinate System (GCS). They instead use SWEREF 99 which stands for Swedish Reference Frame 1999 which is not easily translated to GCS coordinates. Another method that could have been used was to gather speed limit points from the Google API Roads API. Although this could have saved time gathering the necessary points, this API requires a Google Cloud console premium plan. Due to the cost of this, it was decided to instead use NVDB and locate the points manually.

After gathering the points for all the routes from Chalmers University of Technology to Uppsala University from NVDB the SWEREF 99 coordinates were converted to GCS coordinates. This was done using the following code and the resulting coordinates were saved to a CSV file stored locally.

```
import pandas as pd
import pyproj

def main(easting, northing):
    # Define the projection systems
```

```
    sweref99_tm = pyproj.CRS.from_epsg(3006)
    wgs84 = pyproj.CRS.from_epsg(4326)

    # Create a transformer object
    transformer = pyproj.transformer.Transformer.from_crs(
   sweref99_tm, wgs84)

    # Convert SWEREF99 TM to latitude/longitude
    latitude, longitude = transformer.transform(easting, northing)

    return latitude, longitude

# Will run when running the script
if __name__ == '__main__':
    # Define dictionary to stor GCS coordinates
    lat_long = {'lat':[], 'long':[]}
    # Read the csv file with SWEREF 99 coordinates and assign it to
    a pandas dataframe
    df = pd.read_csv(r'C:\Users\Jakob\Desktop\Chalmers\Kandidat\
   Datainsamling\road_data.csv')
    for i in range(len(df)):
        # Gather GCS coordinates and store it in the dictionary
        lat, long = main(df['easting'][i], df['northing'][i])
        lat_long['lat'].append(lat)
        lat_long['long'].append(long)
    # Store the GCS coordinates in the pandas dataframe
    df['latitude'] = lat_long['lat']
    df['longitude'] = lat_long['long']
    # Write and convert the dataframe to the csv file stored
   locally
    df.to_csv(r'C:\Users\Jakob\Desktop\Chalmers\Kandidat\
   Datainsamling\road_data.csv', index=False)
```

Listing 3.1: Converting SWEREF 99 coordinates to GCS coordinates.

3.1.2.2 Gradient

After the GCS coordinates were established data for elevation, next and previous points, next chargers, road distance to the next point, and gradient to the next point could be collected. Both elevation and road distances to the next points were gathered using API's from Google. (The road distances were stored in kilometers). The next and previous points were manually written by locating which points come after the other on the given route. Lastly, the gradient to the next point was calculated using the following equation where the distance unit is in kilometers and elevation in meters:

$$Gradient = \arcsin\left(\frac{elevation_{current} - elevation_{next}}{distance \cdot 1000}\right) \tag{3.1}$$

This was implemented for all the respective points using a Python script.

3.1.2.3 Detour to charging station calculations

Once the points for speed limit changes on all three routes had been determined with the corresponding information about elevation difference, the distance between them, and their speed limit, the next step was to find out how the detours to each charging station would look like from the main road. This was a difficult step since the collected data was of the type GCS. In order to make the process smooth, a visualization using Google's API and creating a website in HTML and Javascript was made to see which charging station or stations were located in between each speed limit change. Markers for every charging station location were placed on the map with the corresponding name and markers for speed limit changes, as can be seen in Figure 3.1.

Once the points were placed on the map, Google's API was used once again to find the best route and display it on the map. By doing so, the road could easily be tracked visually, and once there was a charging station between two speed limit changes, the GCS coordinates for the nearest highway exit was found and placed in the CSV file. This was done for all three routes so that the distance and elevation could be calculated and stored for every charging station detour.

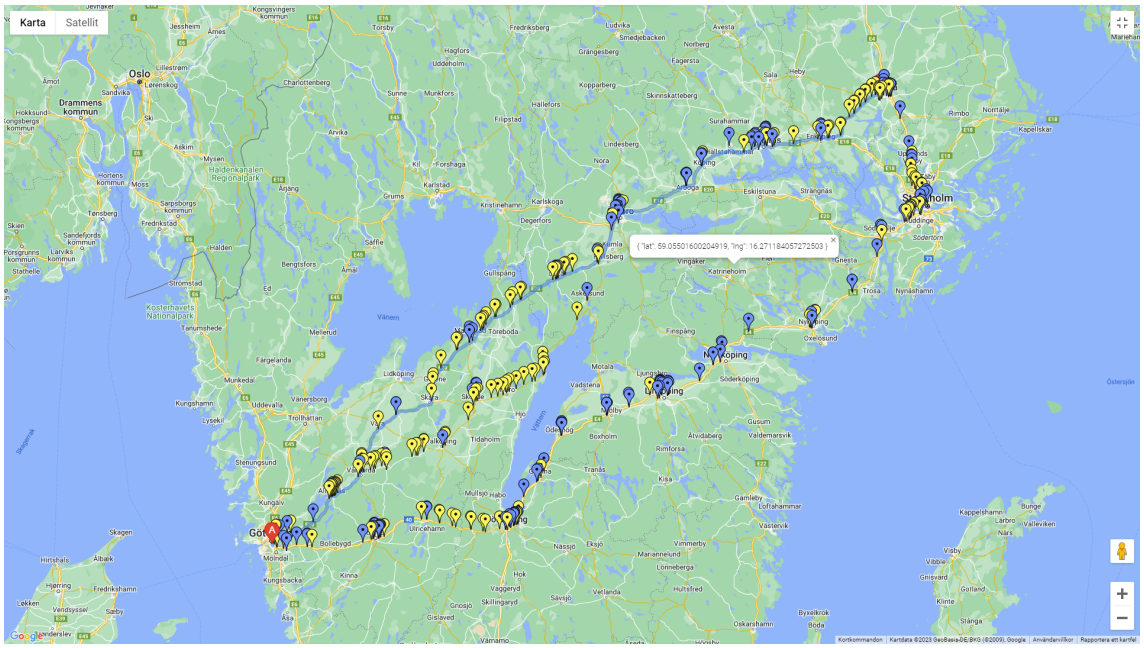

Figure 3.1: Map of charging stations (blue), speed limit signs (yellow), and the fastest route

3.1.2.4 Structuring data

A crucial part for the algorithm to work as intended, the data gathered would need to be structured in a way that supports the procedure of the algorithm and also for easy comprehensibility for users. At first, a single CSV file was used to store all the road data including every single route. This would later turn out to be problematic when calculating energy use and vehicle dynamics properties and also for compre-

hensibility as the points split into different routes into several occasions. For this to work, the columns representing the next point's properties would need to contain more than one value, and the algorithm would therefore need to know which of these values corresponds to which route, further increasing the complexity in which the algorithm operates. To combat this issue, the three different routes were split into their own separate CSV file where every next point property would correspond to only one next point on the route and could be handled by the algorithm separately. The header of the CSV files can be shown in Figure 3.2

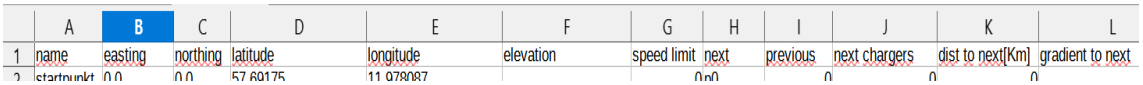

	A	B	C	D	E	F	G	H	I	J	K	L
1	name	easting	northing	latitude	longitude	elevation	speed limit	next	previous	next chargers	dist to next[Km]	gradient to next
2	startpunkt	0.0	0.0	57.69175	11.978087		0.00		0	0	0	

Figure 3.2: A picture showing the column names of the CSV files.

3.1.3 Collecting data of charging behavior

The underlying data used to calculate the parameters of the charging process later described in Section 3.3.1 was conducted by Bjørn Nyland [46], a Norwegian who is well known for his in-depth reviews, tests, and comparisons of different BEV models. Among his assessments are range tests, acceleration trials, and charging power examinations during charging. The data he gathers is publicly available, including his collection of charging data for a range of vehicles, providing the charging power in kW for each level of SoC whilst charging. The file contains 72 charging tests of different BEVs. A small snippet of the data can be seen in Figure 3.3 below. The data was downloaded as a CSV file and 69 tests remained after excluding those that failed to meet the charging duration criterion ($20 \leq SoC \leq 80$) and those that did not specify the charging vehicle. A new row was created with the corresponding battery capacity for every vehicle visualized in Figure 3.4.

A	B	C	D	E	F	G	H	I	J	K	L	M	N	O	P
SoC	Tesla Model Y LR LG Aug 2021	Tesla Model Y LR LG April 2022	Tesla Model Y LR LG April 2022 cold	Audi e-tron 55 new 85.7 kWh	Polestar 2 78 kWh	Polestar 2 64 kWh	Tesla Model S P85 2013	Porsche Taycan 93 kWh	Tesla Model 3 LR 80 kWh Panasonic	Mercedes EQC	Jaguar I-Pace	Hyundai Ioniq 28 kWh	Kia e-Soul 64 kWh	Audi e-tron 50	Volvo XC40 69 kWh April 2022
10	200	250	122	138	130	110	110	250	250	104	94	62	67	125	131
11	191	246	133	138	132	110	105	252	250	105	98	62	67	125	131
12	187	233	126	139	133	112	100	252	250	105	94	62	67	125	131
13	181	220	118	140	137	113	96	253	250	106	94	62	67	125	132
14	175	211	115	141	140	113	92	254	250	106	94	62	68	126	133
15	172	200	112	141	143	113	90	254	250	106	94	62	68	125	133

Figure 3.3: Data collected

	A	B	C	D	E	F	G
1	SoC	Tesla Mod	Tesla Mod	Tesla Mod	Audi e-trc	Polestar 2	Polestar 2
2	Capacity	72	72	72	85.7	78	64
3	10	200	250	122	138	130	110
4	11	191	246	133	138	132	110
5	12	187	233	126	139	133	112
6	13	181	220	118	140	137	113
7	14	175	211	115	141	140	113
8	15	172	200	112	141	143	113
9	16	167	197	112	142	146	114
10	17	164	193	111	142	148	114
11	18	158	190	110	143	149	114
12	19	159	188	109	142	144	114
13	20	153	183	108	142	146	114
14	21	152	179	107	143	147	114
15	22	150	175	105	143	147	115
16	23	148	172	105	143	144	115
17	24	146	171	104	143	145	115
18	25	145	167	104	143	139	115
19	26	144	165	102	143	141	115

Figure 3.4: Modified data

3.2 Longitudinal vehicle dynamics model

An essential aspect of achieving successful route planning using the tool is to define mathematical models that describe the factors affecting the energy consumption of the vehicle. This enables one to comprehend the potential range per charge and identify the instances when additional charging is necessary. Additionally, it is imperative to establish a model for the battery temperature rate and the heat losses, as well as a model for the discharging rate. Each equation presented in the following sections is evaluated at every data point by means of a Python script. To align the structure of the data points with the equations introduced earlier, the ones presented in power W were converted to energy J by applying the appropriate conversion factors. Below is a table incorporating specific vehicle data needed to construct the longitudinal vehicle dynamics model for the Volvo XC40 Recharge [49].

Model	Volvo XC 40 Recharge (FWD)
Vehicle mass, m	2188$[kg]$
Frontal Area, A_f	2.56 $[m^2]$
Aerodynamic drag coefficient, C_d	0.0329
Battery mass, m_b	312 $[kg]$
Usable battery capacity	69 $[kWh]$
Battery architecture	108s3p
Length	4.40 $[m]$
Rolling resistance coefficient, C_r	0.015

Table 3.1: Volvo XC 40 Recharge data sheet.

3.2.1 Propulsion module

With the necessary data collected for the designated road data points and the relevant equations presented in Section 2.2, an energy consumption model due to the propulsion of the vehicle was constructed. This model encompasses the two states of driving, namely acceleration and constant velocity. To simplify the simulation, it was decided that assuming a constant acceleration that appropriately aligns with the speed limits would be sufficient to deduce the resultant force on the vehicle. It was also determined that adding a percentage to the energy drawn during driving would be sufficient to model potential tyre slip.

In order to replicate the acceleration of an XC40 Recharge, data was collected regarding its acceleration times between various speed limits while driving full throttle [47]. To simulate a more typical driving style, these times were subsequently multiplied by a factor of four. From the acceleration times, a constant mean acceleration could be derived using the following equation, where k stands for the current data point.

$$a_{tot} = \frac{v_{k+1} - v_k}{\Delta t} \tag{3.2}$$

With the resulting acceleration for the vehicle between all data points a resulting force could be computed utilizing equation (2.4). This was then used to determine the power output required from the electric motor, employing equations (2.4) and (2.5). To accurately emulate the energy consumed by a BEV a model of regenerative braking is crucial. This was done by assuming that all the braking was done regeneratively within the constraints of a modern regenerative braking system, these were mentioned in Section 2.2.2.

$$E_{acc} = \frac{(F_{tot} + F_{air} + F_{roll} + F_{gradient}) \cdot D_{acc}}{\eta_{losses}}, \qquad [0 < a_{tot} \qquad] \quad (3.3)$$

$$E_{acc} = (F_{tot} + F_{air} + F_{roll} + F_{gradient}) \cdot D_{brak} \cdot \eta_{losses}, \qquad [-2.9 < a_{tot} < 0[m/s^2]] \quad (3.4)$$

$$E_{acc} = 0, \qquad [\quad a_{tot} < -2.9[m/s^2]] \quad (3.5)$$

η_{losses} denotes a combined efficiency factor that accounts for all the energy losses obtained while converting the chemical energy from the battery cells of the battery pack to propel the vehicle forward. D_{acc} refers to the distance covered while accelerating. Finally, to replicate the consumption while driving at constant velocity the same equation used under acceleration was used with the only difference being that $F_{tot} = 0$ and D_{const} which refers to the distance driven while maintaining constant velocity.

$$E_{const} = \frac{(F_{air} + F_{roll} + F_{gradient}) \cdot D_{const}}{\eta_{losses}} \quad (3.6)$$

To conclude the energy consumed at each data point the two driving states were summed together. Additionally, a slip loss factor was incorporated to account for the energy lost due to the slip. It was derived from the results of B.Gao, et al [36] which simulated the energy loss due to slip for a 4WD electric vehicle. They concluded that the loss equals approximately 5% of the total energy consumed due to propulsion forward.

$$E_{drive} = (E_{acc} + E_{const}) \cdot sliploss \quad (3.7)$$

3.2.2 Thermal module

Having developed the energy consumption model, the subsequent step was to develop a mathematical model describing the temperature rate of the battery pack and the heat losses occurring. This is crucial as it enables the application of proper thermal management to optimize performance. By integrating the heat transfer mechanisms presented in Section 2.4.1 and considering the first law of thermodynamics, stating that "energy cannot be created or destroyed", it is possible to manage the temperature change of the battery pack. Initially, the decision was made to assume that the temperature is uniform throughout the battery pack. This approach was selected to simplify the temperature management for each battery cell since they are the subject of performance loss if not kept at optimal temperature. The problem with this approach is that the specific heat capacity C_p of the battery pack is rather complex

to determine. The specific heat capacity quantifies the amount of heat needed to increase the temperature of one kilogram of the object by one kelvin. It was chosen accordingly to the study done by Batterydesign.com [20] which presented a range of 800-1100 $J/kg \cdot k$. Based on this assumption, an energy balance over the battery pack as one homogeneous unit is sufficient. The energy balance can be seen visually in Figure 3.5.

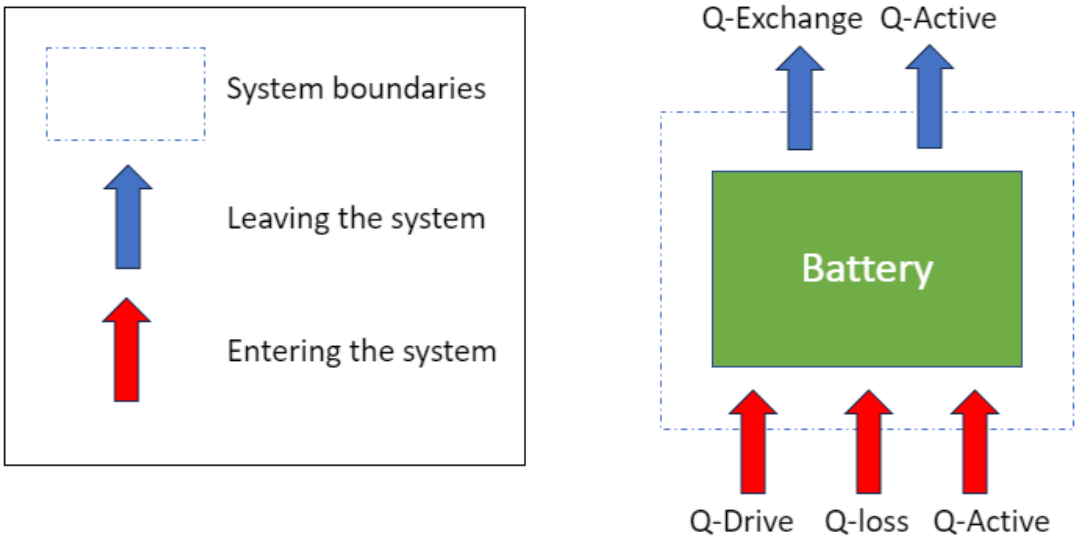

Figure 3.5: Energy balance over battery pack

From the energy balance the dynamic temperature rate $\dot{T}_b$ for the battery can be derived, see the equation below.

$$\dot{T}_b = \frac{Q_{Drive} + Q_{loss} + Q_{Active} - Q_{Exchange}}{C_p \cdot m_b} \tag{3.8}$$

- $Q_{Exchange}$: Refers to the passive heat transfer between the battery pack and the ambient air.
- Q_{Active}: Denotes the quantity of thermal energy applied or transferred from the chosen thermal management system.
- Q_{Drive}: Accounts for all the heat generated as a result of mechanical losses while driving. Derived as 3% of the total energy consumed while driving.
- Q_{Loss}: Heat transferred due to the ohmic resistance losses that occur while the battery is under load.

In order to establish the thermal module, a thermal data sheet as seen below has been compiled from various sources presented throughout the report, containing essential data.

Prandtl number, P_r	0.7362
Dynamic air viscosity, μ_{air}	$1.729 \cdot 10^{-5}$ $[Ns/m^2]$
Thermal conductivity air, k_{air}	0.02364 $[W/m \cdot K]$
Reynolds number, R_e	$4.11 \cdot 10^5$
Ambient temperature, T_a	0 [°C]
Air density, ρ_{air}	1.292 $[kg/m^3]$
Battery starting temperature, T_b	0 $[°C]$
Battery specific heat capacity, C_p	900 $[J/kg \cdot K]$
Length of battery, L_b	2.75 $[m]$
Width of battery, W_b	1.5 $[m]$
Efficiency HVCH, η_{hvch}	87 [%]
Efficiency HVAC, η_{hvac}	87 [%]
Power HVCH, P_{hvch}	2500 $[W]$
Power HVAC, P_{hvac}	2500 $[W]$

Table 3.2: Thermal Datasheet.

3.2.2.1 Leaving the system

When evaluating the heat leaving the system it is important to consider the passive heat exchange with the ambient air and the heat actively transferred away due to a thermal management system. In the context of a battery pack of a BEV, all three heat transfer mechanisms must be assessed in passive cooling. Conduction takes place through the interface between the battery pack and the chassis of the vehicle, convection occurs due to the circulating airflow surrounding the pack, and heat is emitted due to radiation from all objects. To simplify and make the model more manageable the contribution of conduction is neglected. This is based on the argument that modern battery packs are typically well insulated and the heat leaving the pack via conduction is minimal. Furthermore, radiation can also be neglected if the temperature limits of the battery are upheld, as the temperatures where radiation becomes significant will not be attained. With these assumptions $Q_{Exchange}$ can be modeled with the simple equation for the case of convection, see equation (2.15). The equation for this specific case can be seen below.

$$Q_{Exchange} = 2 \cdot h_{convection} L_b W_b (T_b - T_a) \cdot t_{drive} \tag{3.9}$$

$L_{battery}$ and $W_{battery}$ are the length and the width of the battery pack exposed to the ambient and hence subject to convection. The length of the battery exposed is approximated by subtracting the diameter of the wheelbase from the total length of the BEV studied and the width is assumed to be equal to the width of the vehicle. Factor two is to account for both sides of the pack. The specific convection scenario must be defined to evaluate $h_{convection}$. In this case, the decision was made to assume forced laminar convection over a flat plate. This results in the following equations being used [37].

$$N_u = 0.0664 R_e^{1/2} P_r^{1/3} \tag{3.10}$$

To confirm whether the airflow is laminar the Reynolds number must be checked using equation (2.18). The dynamic viscosity and density were obtained from table A.4 in Incopera [37] with the temperature of the ambient air. Furthermore, the velocity of the flow was approximated to $2m/s$ since this is the average velocity produced within the cabin compartment during spring and summer weather by low fan settings while a car is moving between $10 - 100km/h$ [50]. The assumption turned out to be correct, the airflow is laminar and the $h_{convection}$ could then be computed using equation (2.16).

The active heat dissipation was simulated using a constant power multiplied by an efficiency factor to replicate a simple cooler. The primary objective of the cooler was to prevent thermal runaway and optimize performance by keeping the temperature below $45°C$. The power consumption and efficiency of the onboard cooler have been derived from the results of A. Hamendia [21], the equation employed in this context is presented below.

$$Q_{active} = -\eta_{hvac} P_{hvac} \cdot t_{active} \tag{3.11}$$

3.2.2.2 Entering the system

The battery pack's temperature is influenced by three significant heat-generating components, comprising of one active and two passive sources. The active component is an onboard battery heater designed to activate once a suitable charger is detected. Its purpose is to precondition the battery to approximately 20°C, minimizing internal resistance and enabling higher power charging rates. The model was conducted using the same principle as that of the cooler, but in this case, the heat was transferred to the battery instead of being dissipated from it.

$$Q_{active} = \eta_{hvch} P_{hvch} \cdot t_{active} \tag{3.12}$$

Passive sources also contribute to the battery pack's heat generation when driving, mainly through mechanical losses and internal ohmic resistances in the battery. The Q_{Drive} term represents a percentage of the mechanical and electrical power losses (η_{losses}) encountered during the route. The percentage was estimated due to the difficulty in obtaining precise values, by attempting to reproduce the results of previous work on optimal thermal management by Ahad, H [21]. The estimation yielded $\eta_{Qdrive} = 20\%$, resulting in the following equation:

$$Q_{Drive} = \eta_{Qdrive} \cdot (1 - \eta_{losses}) \cdot E_{drive} \tag{3.13}$$

The final passive heat mechanism is the irreversible heat losses (Q_{loss}) resulting from internal ohmic resistance generated by the ion flow within the battery cells. When computing Q_{loss} for the complete battery pack, it's essential to consider the contribution of each battery cell connected in series (n_{series}). The following equation illustrates Q_{loss}:

$$Q_{loss} = R_b \frac{E_{drive}^2}{(n_{series} \cdot {U_{oc}}^2)} \tag{3.14}$$

3.2.3 Discharge module

To conclude the mathematical modeling of the vehicle the last step was to describe how the energy consumed affects the SoC of the battery. As stated in Section 2.3.1 the discharge rate is dependent on the power consumed, the total capacity of the battery, and the UoC. While the power consumed can be derived from the energy model and thermal model respectively the total capacity of the battery was available from Volvo[49], the UoC, however, is not publicly available. Due to the limited information provided by Volvo about the battery pack, a linearized UoC-function was fitted using the data presented in Figure 2.4. The function was fitted between $20-80\%$ SoC since it behaves more linearly in this region and also as these were the specified boundaries for the model, see equation (3.8) for the full function and Figure 3.3 for a visualization.

$$U_{oc} = \frac{\Delta Uoc_{max,min}}{\Delta soc_{max,min}} \cdot soc + 3.43 \tag{3.15}$$

$$U_{oc} = 0.00583 \cdot SoC + 3.43 \tag{3.16}$$

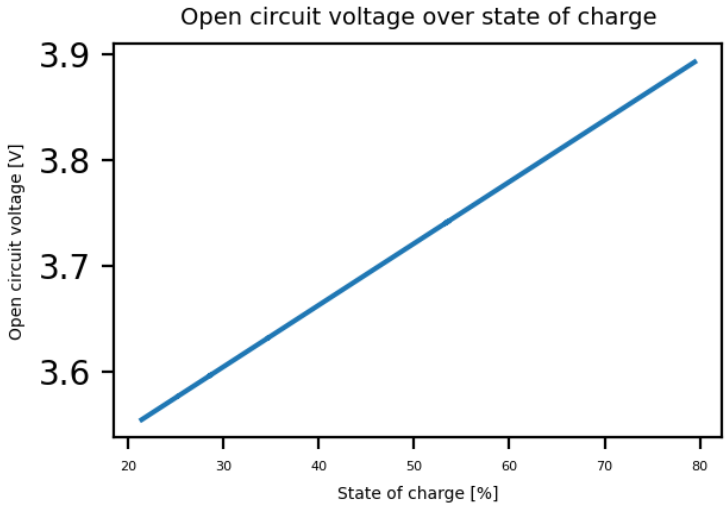

Figure 3.6: Linear representation of U_{oc} depending on the current SoC

After establishing a function for the UoC the rate of discharge could be derived with the following equation.

$$S\dot{o}C = \frac{E_{drive} + Q_{loss} + Q_{active}}{C_b U_{oc}} \tag{3.17}$$

3.3 Charging modelling

3.3.1 Charging time

Modeling a BEVs time to charge (TTC) is a challenging task due to the wide range of factors that affect it, including battery capacity, charging power, SOC, temperature, battery chemistry, charging infrastructure, and so on. Therefore, an accurate estimation requires extensive data from the given vehicle and charging stations, as well as an understanding of how the power grid is impacted by multiple BEVs charging simultaneously. However, acquiring such data is difficult, and relying on a limited number of data points can lead to significant deviations from reality. As a result, the approach was to gather as much data as possible regardless of what vehicle was charging and what the infrastructure looked like. It was determined that a reliable model could be made by solely looking at data on how the charging power to the BEV changed over time for every SoC.

3.3.1.1 Deriving the TTC Equations

The general equation for the time it takes to charge is given as:

$$t = (SOC_{Max} - SOC_{Initial}) \cdot \frac{E}{P} \tag{3.18}$$

where E is the energy capacity of the battery (kWh) and P is the power provided (kW) from the charger. Since the power provided varies for every SOC, the total time will be given as the sum of every time step:

$$t = \Delta t_1 + \Delta t_2 + \Delta t_3 + ... + \Delta t_k \ , \ \Delta t_k = \frac{E_k}{P_k} \tag{3.19}$$

and:

$$E_k = E_{final} - E_{initial} = \frac{E}{100} \cdot \Delta SOC \ , \ \Delta SOC = 1 \tag{3.20}$$

which gives:

$$TTC = \sum_{i=0}^{n} t_i = \sum_{i=0}^{n} \frac{E_i}{P_i} = \sum_{i=0}^{n} \frac{E_i}{P_i} \ , \ i = SoC_{initial} \ and \ n = SoC_{end} \tag{3.21}$$

The energy required for every SoC E_i in equation (3.21) does not take the energy loss whilst charging into account. Thereby, equation (3.17) was modified and implemented into the TTC calculations:

$$Q_{loss,i} = R_b(T_{b,i}) \cdot (\frac{P_i}{U_{oc}(i) \cdot n_{series}})^2 \cdot \mu \tag{3.22}$$

$$\dot{T_b} = \frac{Q_{loss,i}}{C_p m_b} \tag{3.23}$$

$Q_{loss,i}$ is the heat generated for a given SoC, $\dot{T_b}$ is the increase in temperature and $\mu = 2.78 \cdot 10^{-7}$ is a convertion constant from joules to kWh. This gives the final

equation for the TTC, total energy loss, and final temperature of the battery assuming the battery charges from 20 to 80 %:

$$TTC = \sum_{i=20}^{80} t_i = \sum_{i=20}^{80} \frac{E_i}{P_i} = \sum_{i=20}^{80} \frac{E_i + Q_{loss,i}}{P_i} \tag{3.24}$$

$$Q_{loss,tot} = \sum_{i=20}^{80} R_b(T_{b_i}) \cdot (\frac{P_i}{U_{oc}(i) \cdot n_{series}})^2 \cdot \mu \tag{3.25}$$

$$\dot{T}_{b,tot} = \sum_{i=20}^{80} \frac{Q_{loss,i}}{C_p m_b} \tag{3.26}$$

3.3.1.2 Charging Time Calculation Implementation

The TTC for each test was calculated after formulating the corresponding calculations. In order to accurately calculate the total energy consumption during the trip and account for the vehicle dynamic models, the battery's energy loss and temperature were crucial factors that were stored for each test. The initial battery temperature was assumed to be 20 C° for each test as the BEVs heating and cooling system should regulate the battery temperature to be 20 C° prior to charging.

In order to pair each time series with a corresponding charger, the maximum charging power delivered during charging was used as an approximation since the data did not specify the actual charger power. This meant that a time series for a certain car could be associated with a 147 kW charger even though it in fact was a 150 kW charger. However, the deviation is assumed to be small enough to not have a significant impact.

A CSV file with the corresponding time for every SoC was created and the total time to charge was put in a list. In order to apply the collected data to the Volvo XC40 Recharge 69 kWh battery, it is assumed that the time required to charge a battery is proportional to the battery's capacity.

$$t_{new} = \frac{Charging\ \ capacity(VolvoXC40)}{Charging\ \ capacity(Data)} \cdot t \tag{3.27}$$

The equation gives a good estimate of the relationship but is not completely accurate. As earlier mentioned, the battery chemistry also affects the TTC, hence also the relationship between two batteries charging time.
The Implementation and structure of the code can be seen in the flowchart (Figure 3.7). The predictive subroutines denoted in the flowchart will be mentioned in the next section.

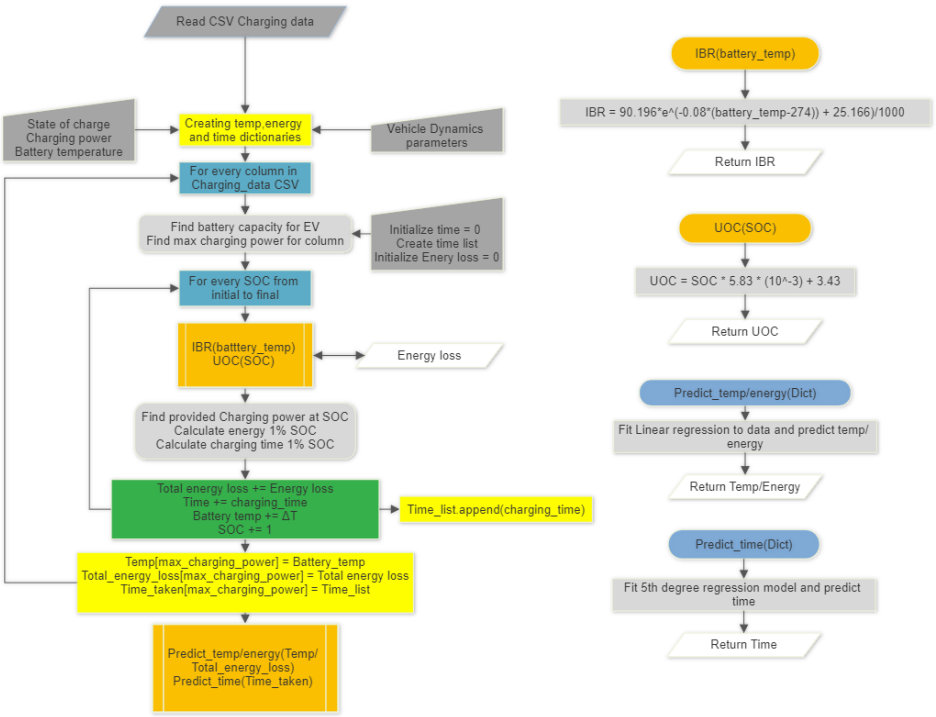

Figure 3.7: Flowchart of code implementation

3.3.1.3 Prediction of TTC

When plotting the TTC as a function of charge power, as seen in Figure 3.8, the data points are quite widespread. Looking at the 150 ± 10 kW range, for example, the charging time varies from roughly 0.3 to 0.65 hours. This is not a surprise, since there are so many factors affecting the TTC and accurate estimation would require more precise data. If there was a lot of data from the Volvo XC40 recharge under given conditions, the relationship between TTC and charge power would have more distinct linear behavior.

In order to fit the non-linear data, a polynomial regression model was used, results can be seen in Figure 3.9. By using a higher-order polynomial term, in this case of the 4th degree, the model fitted the data more closely as it had increased flexibility. It was implemented using the built-in NumPy function polyfit (Listing 3.2) which uses the least squares method to find the best-fit 4th-degree polynomial with coefficients $[a, b, c, d, e]$. Using a higher-degree polynomial resulted in overfitting of the data which occurs when the model learns the noise or random fluctuations of the data rather than following the relationship between the variables.

$$TTC = ax^4 + bx^3 + cx^2 + dx + e \tag{3.28}$$

```
import numpy as np
p = np.polyfit(charge_power, time_to_charge, 4)
```

Listing 3.2: Fitting regression model

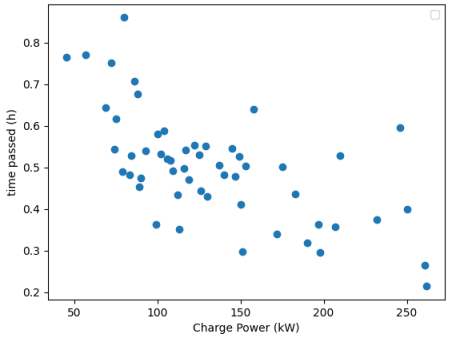

Figure 3.8: TTC for given Charge power

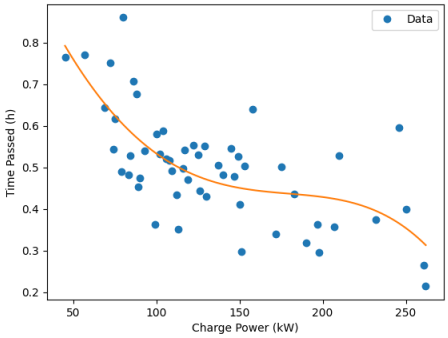

Figure 3.9: Polynomial regression model of 4th degree

3.3.1.4 Prediction of Battery temperature and Energy

As earlier mentioned, the battery's temperature increase and the resulting energy loss while charging are significant parameters. The battery temperature plays a vital role in vehicle dynamics and increases a lot during charging. Hence, a good estimation is of central importance. The energy loss is also of importance as the algorithm takes the energy used into account when planning the route. As seen in the flowchart (Figure 3.7), both parameters are calculated and added to a dictionary for every SoC and charging power. The result is shown in Figures 3.10 and 3.11. When looking at the plots, a clear linear behavior can be seen, especially for charge powers where more data is collected. The deviation is due to the fact that $Q_{loss,i}$ is dependent on the power P_i provided at every instance, which varies for every test even though the charge power is the same. The data is determined to fit best into a linear regression model. Thereby, a linear regression model was implemented using Pythons plug-in sklearn. The fundamentals of the model are very similar to a polynomial regression, as both utilize the method of least squares to determine the best fit. However, the linear regression model specifically aims to establish a linear relationship, represented by $y = kx + m$. See Figure 3.12-3.13 for the linear regression model.

```
from sklearn.linear_model import LinearRegression
model = LinearRegression().fit(x_data, y_data)
```

Listing 3.3: Fitting linear regression model

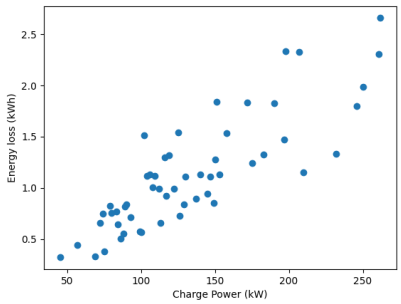

Figure 3.10: Energy loss

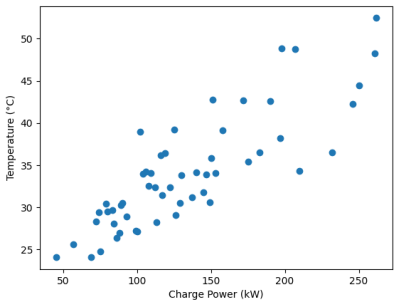

Figure 3.11: Final temperature

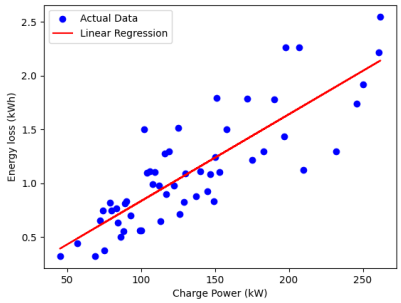

Figure 3.12: Predicting Energy loss

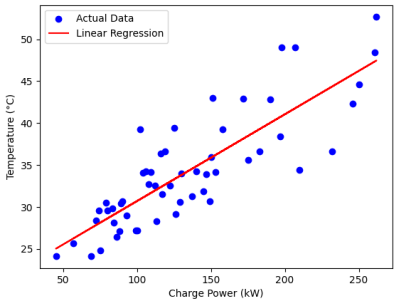

Figure 3.13: Predicting Final temperature

3.3.2 Stochastic modeling of charger availability

Using the Markov chain method as described in Section 2.6, a model is created to describe the availability of charging for each charging station. In this model, the different capacities of each charging station are represented as a discrete Markov chain. The state probability, denoted as $S = [0, 1, ...n]$, represents the number of available chargers, ranging from 0 to n where n is the number of chargers at the station. The transition matrix describes the probability of transitioning from a starting state to a new state.

The data collection process for the number of charging stations, their power output, and their availability is described in Section 3.1.1. The collected data is used to calculate the transition matrices. Each time step during data mining is set at 30 minutes, and the initial starting values are calculated based on the frequency of available chargers. The transition matrices are then calculated according to the number of times the state changed.

The model calculates the time it takes to drive and arrive at a charging station using stochastic variables to estimate the initial number of available charging slots based on prior data. The initial state vector is then multiplied with the corresponding transition matrix, T, a certain number of times x, corresponding to the time it

would take to drive the distance to the charging station. For example, a charging station three hours away would have its initial state multiplied with the transition matrix six times, given that each time step is 30 minutes. The general formula for this calculation is shown in equation (3.29), where m represents the number of time steps needed to reach the charging station, s_{t+m} represents the estimated state, and s_t represents the initial state.

$$S_{t+m} = S_t \cdot T^m \tag{3.29}$$

In practice, this can be seen in Listing 3.4. The class takes as input state, which is the possible amount of chargers a station has, the transition matrix, and initial distribution. The calculation seen in equation (3.29) is defined by the function predict. The output of the process

```
class ChargingStationPredictor:
    """ A Class that runs the availability probability for a given
   station and time interval"""

    def __init__(self, states: list, transition_matrix,
   initial_state_distribution: list):
        self.states = states
        self.transition_matrix = transition_matrix
        self.initial_state_distribution =
   initial_state_distribution

    def predict(self, steps=1) -> list:
        """ a function that runs the state_dist 'steps' number of
   times to calculate the future distribution"""
        current_state_distribution = self.
   initial_state_distribution

        for i in range(steps):
            next_state_distribution = np.dot(
   current_state_distribution, self.transition_matrix)
            current_state_distribution = next_state_distribution

        return current_state_distribution
```

Listing 3.4: Code for the class ChargingStationPredictor which calculates the future availability for a charging station

To reduce the time complexity of the program, all transition matrices and initial values are calculated at the same time at the beginning of the algorithm and stored in a dictionary.

The highest probable quantity of chargers available q_p at the charging station at time t is calculated using equation (3.30), where $p_{i,t}(q_i)$ is the probability of quantity q_i chargers being available at time t and n is the length of the state quantity list:

$$q_p = p_{0,t}(q_0) \cdot q_0 + p_{1,t}(q_1) \cdot q_1 + p_{2,t}(q_2) \cdot q_2 + ... + p_{n,t}(q_n) \cdot q_n \tag{3.30}$$

Thereafter using q_p, the percentage of available chargers p_p is calculated using equa-

tion (3.31), where q_n is the total number of chargers at the charging station.

$$p_p = \frac{q_p}{q_n} \tag{3.31}$$

Finally, the availability cost a_{cost} is calculated using equation (3.32).

$$a_{cost} = p_p \cdot a_{factor} + q_p \tag{3.32}$$

To balance the percentile availability p_p, which has a range of $[0 : 1]$, against the number of chargers q_n, with a range of $[0 : n]$ a multiplier is applied. This availability factor a_{factor} has a value of 3, which was calculated through experimentation.

3.4 Route planning algorithm

Using the previously presented data and models a final algorithm for planning the route was created.

The algorithm goes through each of the three predefined routes described in Section 3.1.2 and tries to choose the optimal charging stations to stop at by minimizing some cost C defined as the sum of all costs c (described in Section 3.4.1) of the charging stations that the vehicle stops at.

Minimizing the final cost of C is simply done by simulating the vehicle up to the points it has to charge. This is defined as all the points where its SoC falls within the range $20 < SoC < 40$. The algorithm then selects the station with the lowest cost among the possible stations the vehicle can stop at given the points its SoC falls within this range and adds it to the list of stations to stop at along the route before continuing the simulation until the vehicle has to charge again.

The simulation of the vehicle is carried out using the method described in Section 3.2 between each of the points on the three defined routes. When it comes to charging a detour route has to be created and simulated. This is done using the data described in Section 3.1.2.3. At the time the algorithm determines the vehicle needs to charge the simulation goes through four additional points. To the closest highway exit, to the charging station's location, back onto the highway, and further to the next point on the route. From here the simulation again uses the points defined on the route until it is time to charge again and a new detour has to be taken by the vehicle. A flowchart of the algorithm can be seen in Figure 3.14.

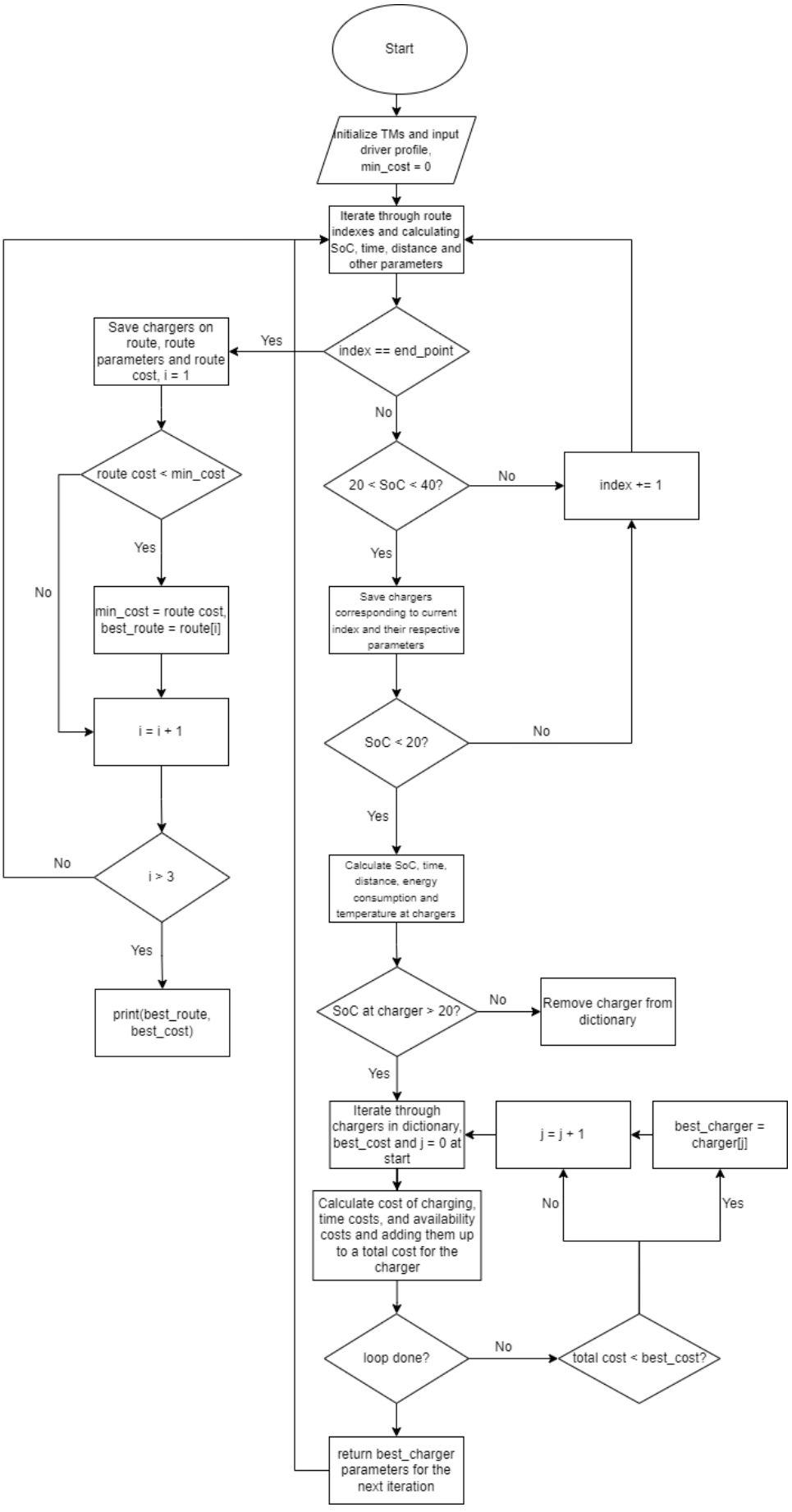

Figure 3.14: A flowchart showing the structure of the route planner algorithm

3.4.1 Station cost function

The cost c_s for each station s is calculated as the weighted sum between the actual price of charging (given a weight of 1) as well as the time it takes to charge given a constant weight t_{cost}. This essentially puts a price on each unit of time. These terms are then further weighted based on a user-defined profile defining custom weights for the price of time, money, and energy.

This sum s_w is then modified using some factor f combining the predicted availability of chargers at station s as well as the vehicles SoC at the charger in order to both penalize charging at a high SoC while also increasing c_s when the availability of the charger is uncertain. The final cost of charging at station s is then

$$c_s = s_w \cdot f \tag{3.33}$$

where

$$s_w = (c_e \cdot p_e) + (t \cdot t_{cost} \cdot p_t) \tag{3.34}$$

$$f = \begin{cases} \infty & \text{if } a_{cost} = 0 \\ \frac{\mathrm{n}(soc_c)}{(80 - soc_c) \cdot a_{cost}} & \text{otherwise} \end{cases} [20 < soc_c < 40] \tag{3.35}$$

and soc_c is the vehicle's SoC (as a percentage) when reaching the charger, $80 - soc_c$ is the required amount soc_c has to increase to reach 80% as the simulation only charges to this amount, $\mathrm{n}(x)$ is a non-linear function penalizing high values of x defined as

$$\mathrm{n}(x) = \begin{cases} \frac{x^2 - 20x}{3} & \text{if } x > 26 \\ 2x & \text{otherwise} \end{cases} \tag{3.36}$$

a_{cost} is a factor based on the predicted availability of the charging station, $a_{cost} \geq 0$, explained in equation (3.32). p_e and p_t are both user-defined weights for the price of energy and the price of time while c_e is the energy price and t is the time spent charging. t_{cost} is arbitrarily chosen to be 10. For more information on the cost calculation see the full code available on GitHub.

4

Results

This chapter contains the key results that were obtained. Firstly is the results of data collection of availability presented, followed by its respective verification methods. Next, the choice of charging stations and then the modeling of the longitudinal vehicle dynamics combined the verification procedures regarding propulsion and thermal management. Additionally, are the results of the charging optimization presented and verified. Finally, the result of the optimization algorithm combining all the components and verified against an existing trip planner.

4.1 Data collection of availability

A program logging availability data of charging stations was successfully developed however the plan to run this program over the course of a month was not carried out. Instead, only minimal data was collected over the period of time between 09/03 18:00 to 10/03 21:00 (2023) because of limitations on the availability of Chargefinder's API which took effect after this logging had occurred and no agreement was able to be made with Chargefinder regarding API access. The average availability of all chargers at a given time according to the data collected can be seen in Figure 4.3. As can be seen, the chargers are most available late at night to early morning with less of them being available midday and the afternoon.

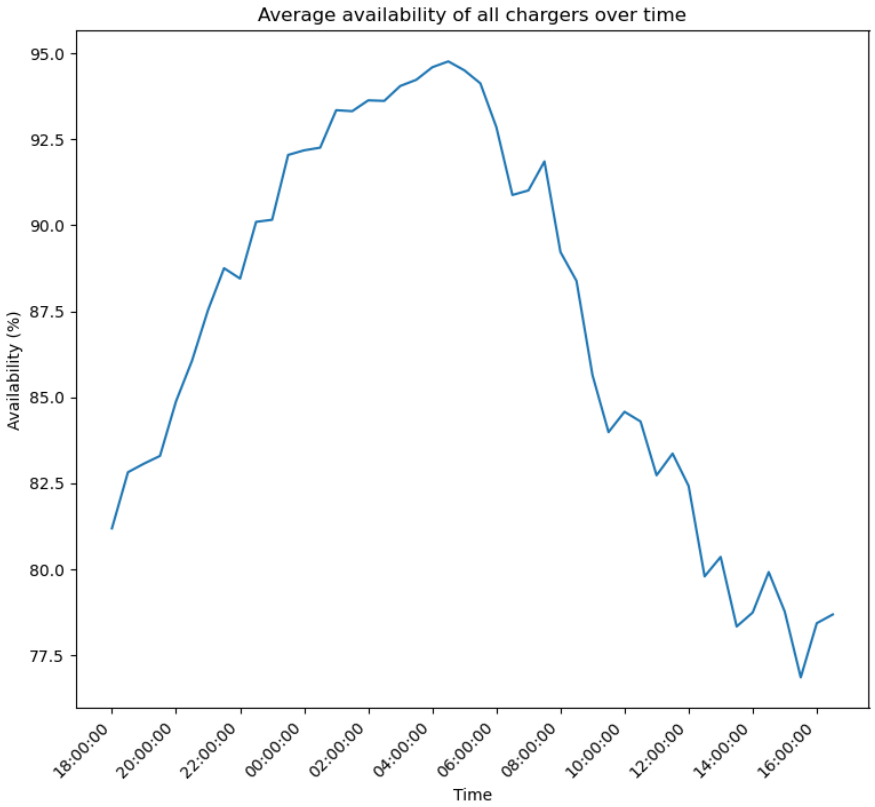

Figure 4.1: Average charger availability

The fact that only a small amount of data was collected means that the program only has minimal usability when it comes to presenting availability as a function of time of day and none when it comes to presenting it as a function of the day as a full week's worth of data was not able to be collected.

Ways of circumventing the loss of API access were considered but not implemented which is discussed further in Section 5.1.1.

4.1.1 Verification of the logging program

The program was verified using unit testing of the various functions. This made sure the program correctly stored and retrieved the information in the database, reading and writing to the id → index dictionary described in Section 3.1.1 correctly as well as reacting accordingly to errors from the server, in particular waiting in the event of a 403 error.

4.1.2 Verification of the logged data

During the development of the logger, there were multiple rounds of making sure the logged data matched the one available on chargefinder.com. After every major change to the code, the final version, in particular, this verification was carried out.

There were no discrepancies between the logged and manually collected data in the final version of the program.

4.2 Choice of charging station

When it comes to the results for specifying stochastic models to plan and prioritize the choice of charging stations along the selected routes the result diverges from the original goal. The original goal was to create a time-dependent Markov chain model where the transition matrices are dependent on the time of day and day of the week. However, due to a lack of collected data from the collection phase of the project which resulted in only two days' worth of data, described in Section 4.1, this could not be achieved in a reasonable manner. Therefore it was decided a more sensible approach was to implement the time-independent Markov chain model which is described in Section 3.3.2.

This time-independent stochastic model works fine. However, the effectiveness of this model is hampered by the limitations mentioned earlier. Due to the scarcity of data and the predominance of nighttime data collection when fewer BEVs are being charged, the transitional matrices do not accurately reflect real-world conditions as much as had been hoped for. Additionally, the small amount of collected data poses another challenge. Some charging stations always have availability or a fixed number of charging posts during the time period when the data was gathered. As a result, their transitional matrices repeatedly point to the same value at each iteration, furthermore reducing the correlation with reality.

4.2.1 Verification of the stochastic model

To test whether or not this stochastic model works as intended, a random charging station on one of the routes was selected. Thereafter the initial state probability distribution and transitional matrix were calculated for that charger and input into the code shown in listing 3.4. The transition matrix T is shown in (4.1).

$$T = \begin{bmatrix} 0 & 0.1 & 0.9 & 0 \\ 0 & 0 & 0.333 & 0.666 \\ 0.0454 & 0.091 & 0.636 & 0.227 \\ 0 & 0.036 & 0.178 & 0.786 \end{bmatrix} \tag{4.1}$$

The initial state probability vector S_0 can be shown in (4.2).

$$S_0 = \begin{bmatrix} 0.018 \\ 0.054 \\ 0.4 \\ 0.527 \end{bmatrix} \tag{4.2}$$

After the predict method from the code in listing 3.4 was executed and the transition matrix was multiplied with the initial state vector 53 times the state probability

reached a steady state S_s, shown in (4.3).

$$S_s = \begin{bmatrix} 0.0167 \\ 0.0551 \\ 0.3672 \\ 0.5609 \end{bmatrix} \tag{4.3}$$

In this case, the initial state vector is already a good approximation of the long-term behavior of the system, and the chain has almost already reached a stable distribution. That is why the probability distribution does not differ that much from the initial state distribution and the steady state distribution vectors.

4.3 Vehicle dynamics modelling

Table 4.1 presents the driving time, distance, and total energy consumption results for the three simulated routes. Henceforth, only the results of the route considered optimal by the algorithm will be presented, the remaining results can be seen in Appendix (A.2-A.7).

	Route 1	Route 2	Route 3
Driving duration [h:m]	5:40	5:33	4:55
Distance [km]	558	491	458
Energy consumption [kWh]	175	141	136

Table 4.1: Result of the longitudinal vehicle dynamics for route 1-3.

The results of the modeling of the route deemed most optimal can be seen in Figure 4.2-4.6. Total energy consumption and SoC over distance can be seen in Figure 4.2-4.3, the red markers indicate a charging stop. Figure 4.4-4.6 shows the battery temperature over distance and time for three different ambient temperatures. The green dotted lines indicate the temperature range $15 - 30°C$, which as mentioned in the previous sections is the most optimal interval when driving. The black dotted line represents 20°C and finally the red marks 45°C which is the upper limit for neglecting thermal degradation.

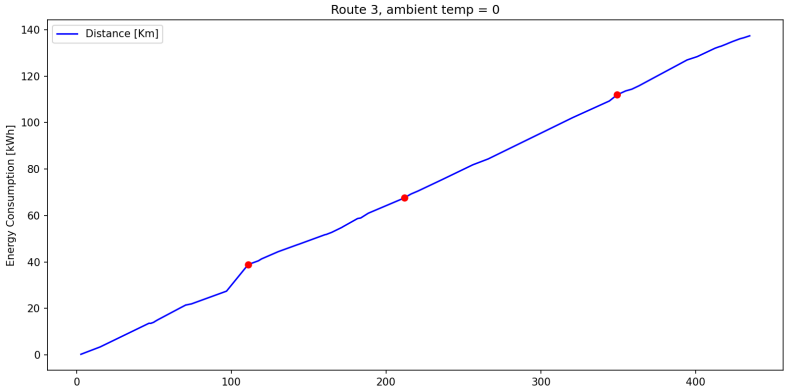

Figure 4.2: Total energy consumption over distance.

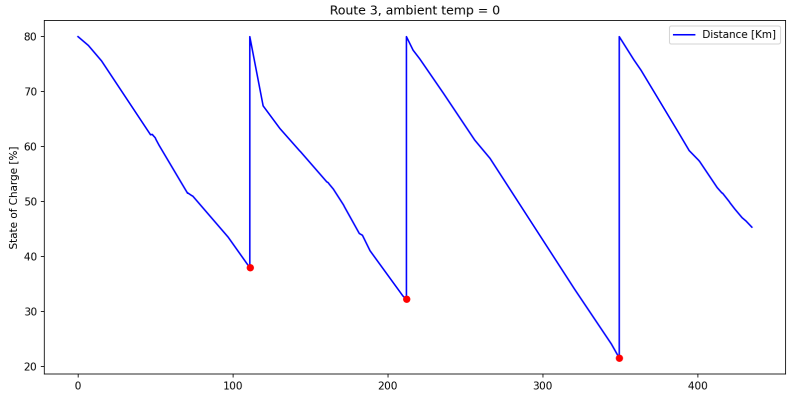

Figure 4.3: SoC over distance.

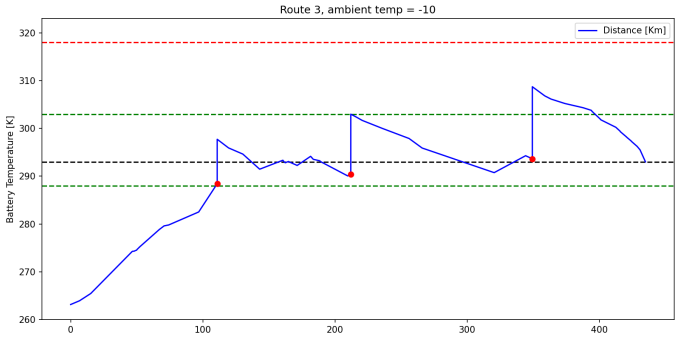

Figure 4.4: Battery temperature over distance at ambient temperature −10°C for route 3

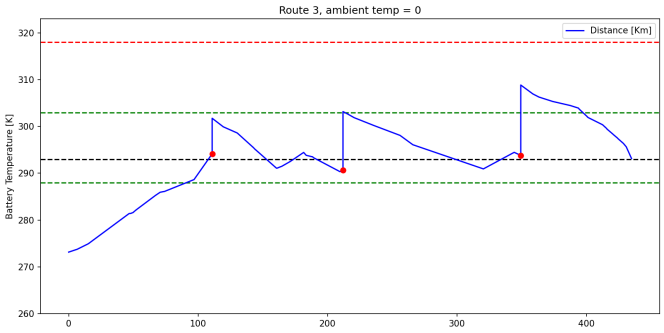

Figure 4.5: Battery temperature over distance at ambient temperature 0°C for route 3.

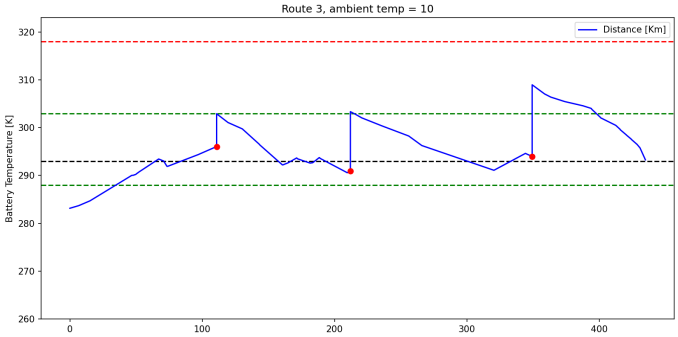

Figure 4.6: Battery temperature over distance at ambient temperature 10°C for route 3.

A verification procedure was conducted to validate the results of the propulsion module and the thermal module, which is elaborated more on in the following sections.

4.3.1 Verification of propulsion module

To validate the results of the propulsion module a projected range was calculated and evaluated with a real-world reference. An estimate of the projected real-life range from 80% - 20% SoC can be attained by utilizing the 75% total real-life range test done in an XC40 Recharge FWD by B. Nygard [46]. The test was performed in dry weather conditions, with an ambient temperature of 17°C and an average

velocity of 90 km/h. The range was then converted into 60% of the total range in order to be compared with the simulated model. The real-life test produced a 60% range of 187.2 kilometers.

The simulated mathematical model with an ambient temperature 0°C and an average velocity of 90.64 km/h equated to a 60% range of 178.7 kilometers. Comparing the real word test to the model results in a deviation of 4.5%.

4.3.2 Verification of thermal module

The thermal module was verified against the simulations of A.Hamednia[21] as represented in Figure 4.7 below. It can graphically be deduced that the simulation for route 3 at -10°C ambient temperature Figure 4.6 behaves similarly for the first 100 km. After the 100 km mark, a few differences can be seen. Firstly A.Hamednia utilizes the onboard heater at 200 km to precondition the battery to 20°C for maximum charging efficiency. Whereas the simulation done by the algorithm already achieves slightly above 20°C temperature before charging without extra heating. In order to compensate for this, cooling by the onboard cooler is activated once the temperature exceeds 30°C in order to keep the battery temperature levels within the optimal driving range of $15°C - 30$°C, and attempting to reach 20°C just before charging.

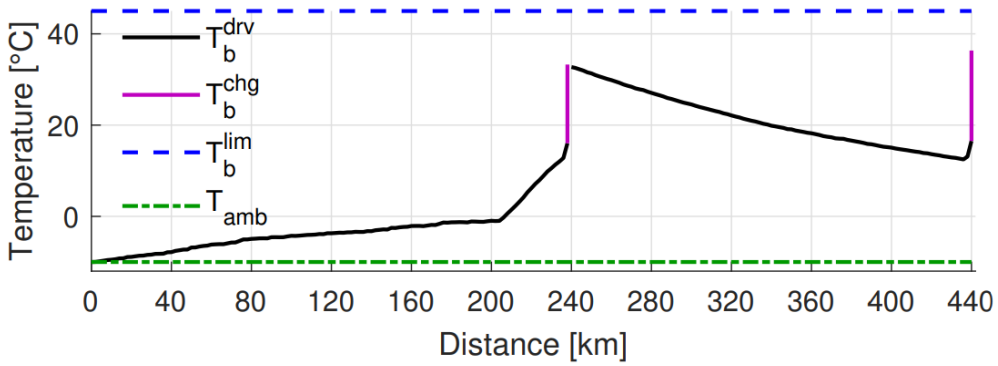

Figure 4.7: Battery temperature over distance. A.Hamednia. *Optimal Thermal Management, Charging, and Eco-driving of Battery Electric Vehicles*[21].

4.4 Charging optimization

The predictive models worked as intended. Given an SoC when reaching the charger and the charger's power, the program returned an estimation of TTC, energy consumption, and battery temperature to the algorithm. In order to verify that reasonable values were obtained from the models, various tests of different starting SoC and charge powers were made (Table 4.2).

Charger (kW)	Starting Soc (%)	TTC (h)	Battery temp (°C)	Energy loss (kWh)
50	20	0.78	25.5	0.43
50	25	0.72	25.2	0.4
50	30	0.66	24.8	0.38
150	20	0.45	35.9	1.2
150	25	0.42	34	1.1
150	30	0.39	33	1.0
250	20	0.38	46	2.0
250	25	0.37	43.5	1.8
250	30	0.35	40.8	1.6

Table 4.2: Testing of model

The results in Table 4.2 were verified by comparing them with existing data and tests. [49] Volvo, in their published technical information for the XC40 Recharge, states that the TTC is 56 minutes for a 50 kW charger and 32 minutes for a 150 kW charger. Nevertheless, they do not specify the SoC interval. Assuming that the vehicle charges from 20 % to 80 %, the predicted data in Table 4.2 suggests that it takes 46.8 minutes for a 50 kW charger and 27 minutes for a 150 kW charger which is very close to the technical data provided by Volvo.

To verify the battery temperature, A.Hamednia [21] simulations were used as a guideline. Figure 4.7 shows a final temperature of about 32 °C. The test was done using a 150 kW charger and a charging interval of 20 % to 62 % SoC. The predicted temperature, charging from 20 % to 80 % SoC (Table 4.2) is 35.9 °C, which is as expected slightly higher.

Verifying the energy loss is difficult as it depends on many factors and extensive data from Volvo would be necessary for the verification. To get a rough estimate, data from B.Nyland [46] was collected, providing the charging loss for a Tesla Model 3 for various charging powers seen in Table 4.3. When comparing these values with the predicted ones in Table 4.2, a significant difference in efficiency can be observed. The largest energy loss predicted was 2.0 kWh, corresponding to a 97 % Efficiency which is significantly high compared to the data. As formulated in Section 3.3.1.2, the predicted energy loss calculated using equation (3.25) does not consider all factors that contribute to the total energy loss during the charging process. These factors include losses from charging cables, power conversions, environmental conditions, and so on. Given the presence of additional sources of energy loss, it was anticipated that the overall charging efficiency would be lower than what was calculated.

Power	Type	Details	Charger +kWh	Battery +kWh	Efficiency	Loss
2.3 kW	AC	10 A 230 V	7	5.9	84.3 %	15.7 %
3.5 kW	AC	15 A 230 V	8.25	7.4	89.7 %	10.3 %
7 kW	AC	30 A 230 V	6.93	6.5	93.8 %	6.2 %
8 kW	AC	11 A 400 V	9	8.2	91.1 %	8.9 %
11 kW	AC	16 A 400 V	15.44	14.1	91.3 %	8.7 %
50 kW	DC	125 A 400 V	11.51	10.9	94.7 %	5.3 %
50 kW	DC	125 A 400 V	13.7	11.3	82.5 %	17.5 %
350 kW	DC	500 A 400 V	33.857	31.1	91.9 %	8.1 %
350 kW	DC	500 A 400 V	57.137	51.9	90.8 %	9.2 %
350 kW	DC	500 A 800 V	81.434	74.734	91.8 %	8.2 %

Table 4.3: Charging loss on Tesla model 3 (B.Nyland)

4.5 Optimization algorithm

The algorithm succeeded in combining the vehicle dynamics, availability distribution, and battery temperature management into a model that calculates the driving time and finds the most reasonable charging stations along the route from Gothenburg to Uppsala that falls in line with the chosen driver profile. The path the algorithm uses can be seen in figure 3.14. The results from running the program can be seen Figure 4.8 and 4.9 which were visualized by constructing a website.

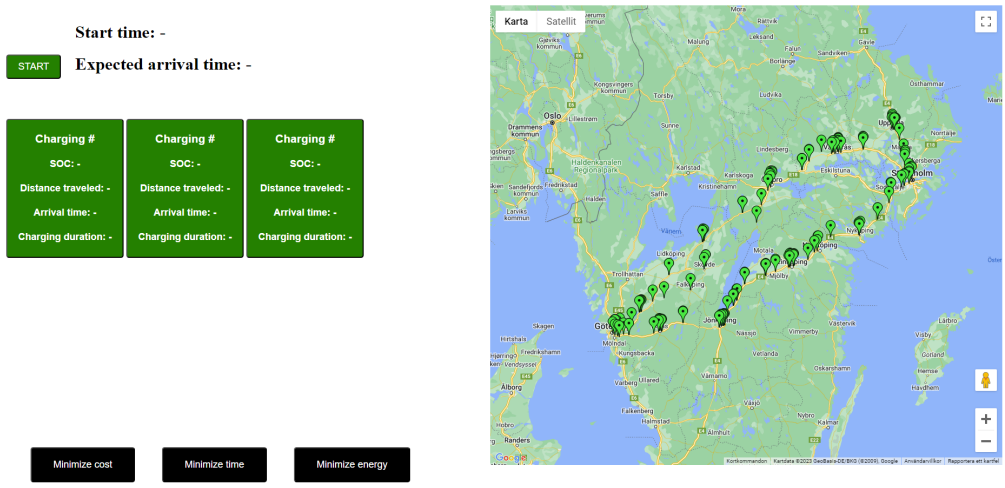

Figure 4.8: Selection of what to minimize and starting time

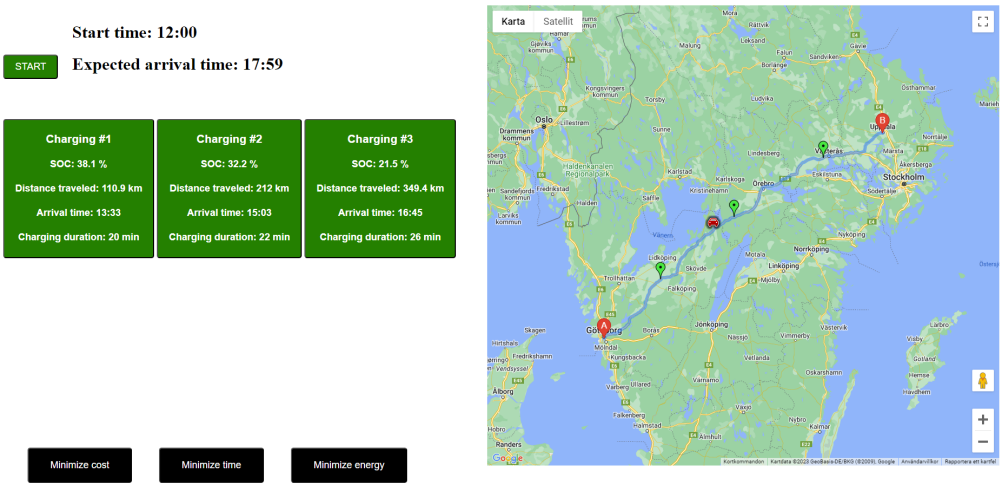

Figure 4.9: Trip planner choosing a route and charging stations. The three green markers represent the charging locations

The result from the three routes can be seen in Table 4.4.

	Route 1	Route 2	Route 3
Total time [h:min]	7:06	6:49	5:59
Driving duration [h:min]	5:40	5:33	4:55
Charging duration [h:min]	1:26	1:16	1:04
charging stops	5	3	3
Energy consumption [kWh]	175	141	136
SoC at destination [%]	37	51	46
cost value	264	255	230

Table 4.4: Result of the algorithm for the different routes

The algorithm determines the most optimal route to be route 3, driving on the E20 past Örebro. The route takes $5h59m$, where the BEV requires charging 3 times, with a total charging time of $1h4m$, and a driving time of $4h55m$. The cost value is the value calculated for driving the route explained in Section 3.4. The chosen charging stations for route 3 and their values are presented in Table 4.5

	Charger 1	Charger 2	Charger 3
Time until arrival [h:min]	1:33	3:03	4:45
Distance traveled [km]	110.9	212.0	349.4
Charging duration [min]	20	22	26
Energy consumption [kWh]	38.87	67.68	111.95
SoC at arrival [%]	38.1	32.2	21.5

Table 4.5: Values for the chargers on route 3

To verify the results of the algorithm, the website "ABetterRouteplanner.com" also known as ABRP was used. ABRP is an existing commercial well-used product,

which is the industry standard in BEV route planning. ABRP's route and values can be seen in Figure 4.10.

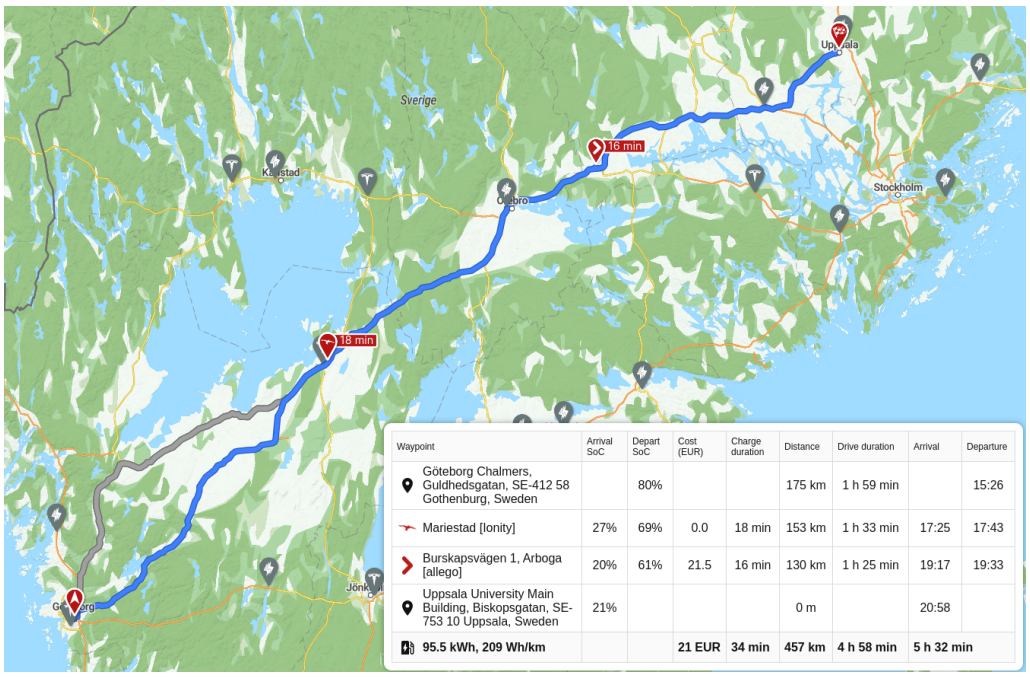

Waypoint	Arrival SoC	Depart SoC	Cost (EUR)	Charge duration	Distance	Drive duration	Arrival	Departure
Göteborg Chalmers, Guldhedsgatan, SE-412 58 Gothenburg, Sweden		80%			175 km	1 h 59 min		15:26
Mariestad [Ionity]	27%	69%	0.0	18 min	153 km	1 h 33 min	17:25	17:43
Burskapsvägen 1, Arboga [allego]	20%	61%	21.5	16 min	130 km	1 h 25 min	19:17	19:33
Uppsala University Main Building, Biskopsgatan, SE-753 10 Uppsala, Sweden	21%				0 m		20:58	
95.5 kWh, 209 Wh/km			**21 EUR**	**34 min**	**457 km**	**4 h 58 min**	**5 h 32 min**	

Figure 4.10: The optimal route according to the website "a better route planner, ABRP", with the original 215 Wh/km @ 110km/h

ABRP selects the same road as the algorithm, with an equal driving time, $4h55m$ vs $4h58m$. The charging time differs a lot, with ABRP only charging twice, for a total charging time of $35m$, while the optimization algorithm chooses 3 chargers, with a charging time of $1h4m$. The discrepancy here probably occurs since the algorithm uses a higher energy consumption than ABRP, with 250 vs $215Wh/km@110km/h$. The energy consumption in the algorithm is derived from sampled data of B.Nygard [46], described in section 4.3.1, while ABRP's is derived from Volvo's official values.

If instead the same energy consumption is used for both cases Figure 4.11, ABRP instead gives the result seen in Figure 4.12.

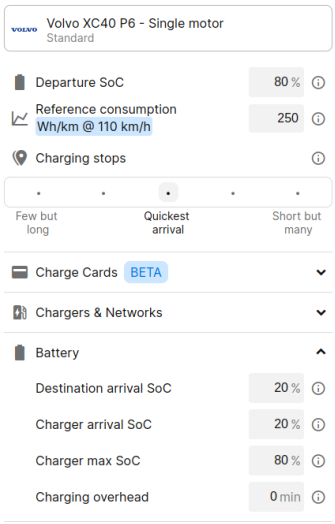

Figure 4.11: Settings for the BEV with energy consumption set to 250 kWh/100 km

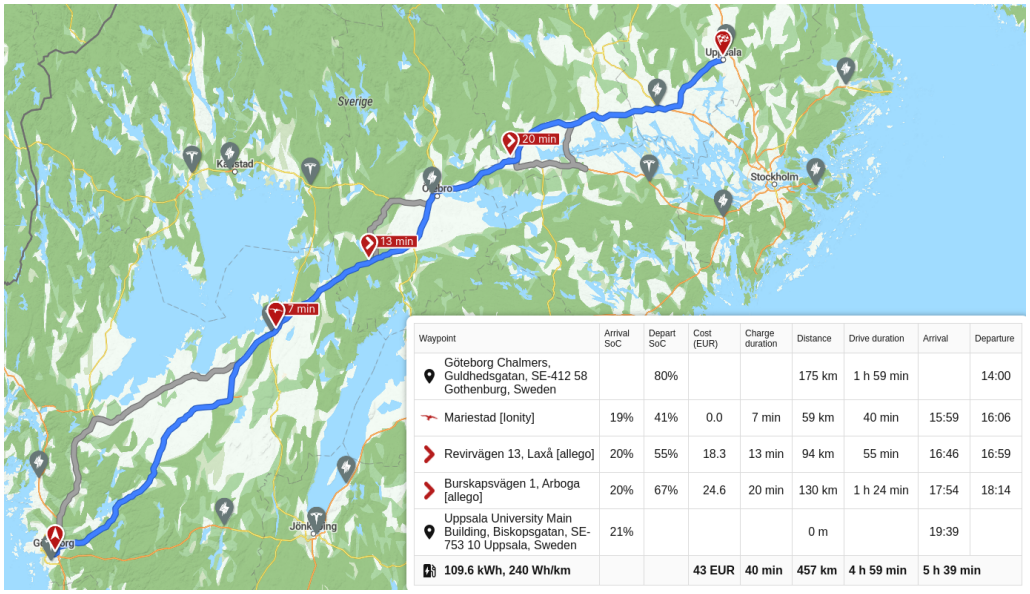

Waypoint	Arrival SoC	Depart SoC	Cost (EUR)	Charge duration	Distance	Drive duration	Arrival	Departure
Göteborg Chalmers, Guldhedsgatan, SE-412 58 Gothenburg, Sweden		80%			175 km	1 h 59 min		14:00
Mariestad [Ionity]	19%	41%	0.0	7 min	59 km	40 min	15:59	16:06
Revirvägen 13, Laxå [allego]	20%	55%	18.3	13 min	94 km	55 min	16:46	16:59
Burskapsvägen 1, Arboga [allego]	20%	67%	24.6	20 min	130 km	1 h 24 min	17:54	18:14
Uppsala University Main Building, Biskopsgatan, SE-753 10 Uppsala, Sweden	21%				0 m		19:39	
109.6 kWh, 240 Wh/km			**43 EUR**	**40 min**	**457 km**	**4 h 59 min**	**5 h 39 min**	

Figure 4.12: ABRP driving with a modified engine of 250 Wh/100 km at 110 km/h

With the updated values, the two models become more closely aligned, both having 3 chargers, but ABRP still has faster charging times. The total energy consumption is still lower in ABRP with 109.6 kWh versus the algorithm's 136 kWh. The difference probably occurs from ABRP not using battery heating and cooling, and relying on producer-given values, which have been calculated in perfect conditions.

5
Conclusion

5.1 Discussion

The discussion section begins by highlighting the problem faced with the data collection process from Chargefinder and its result hindering the creation of accurate stochastic models for charger availability. Additionally, discussed is the limited data on the electricity pricing of the chargers. Furthermore, the inaccuracies of the propulsion and thermal module are presented and their impact on the result is addressed. Next, the discrepancies between the charging model and real-world tests are described, and it is summarized with a conclusion regarding the optimization algorithm and finally future works.

5.1.1 Minimal Chargefinder data collection

Only minimal charging station data was collected because of a change in API policy on Chargefinder's side during the logging. This meant that the API could no longer be accessed directly but only via the website itself. This impacts the accuracy of stochastic models relying on the station availability data which in turn negatively affects the accuracy of the final result. Contacting Chargefinder with a request for API access lead to no response. This could be mitigated by using webscraping in the logger instead of API calls but ultimately that task was determined to be too time-consuming and the problem occurred too late in the project. Doing this would also raise ethical concerns since without an official statement from Chargefinder it would be unclear what they think is acceptable for the group to do with their website even if the data is publicly available.

The inability to access Chargefinder's API also leads to an inability to gather live data for the chargers when running the stochastic availability model. If this data could be collected, the prediction of charger availability could then be run according to the current charging situation by using this as an input for the Markov chain model described in Section 3.3.2.

The lack of data made it impossible to create a time-dependent stochastic model for charger availability. Without the time dependency, much of the usability of the predictive model becomes irrelevant, since it mostly reaches a steady state relatively quickly after only a few iterations. With a time dependency model, the availability forecast would give valuable information to the end user for avoiding busy charging stations during high-capacity time periods.

Furthermore, the loss of API access also means that the algorithm doesn't have access to the electricity price of the chargers. Therefore this has to be predicted based on the charger capacity and does not necessarily reflect the real-world price which further impacts the final result obtained by the trip planner.

5.1.2 Inaccuracies of the propulsion & thermal module

It should be noted that the simulation and the real-life validation test differ in terms of overall energy consumption. Specifically, the simulation does not take into account any auxiliary loads, such as fans, lights, heating, and cooling of the cabin compartment, as it was deemed that including these factors would add unnecessary complexity and only account for a small portion of the energy losses at the simulated ambient temperatures. Therefore, to account for this the efficiency of converting chemical energy into mechanical energy in the simulation is slightly less efficient than it should be. The group allowed for an error margin of 10%, which was achieved and even exceeded by 5.5%. In conclusion, it can be deduced that the propulsion module is close enough to a real-life scenario and provides a solid foundation for the algorithm.

As mentioned in Section 4.3.2 the lack of a complex onboard TMS for the battery pack resulted in a deviation from the results of A. Hamendia [21], which can be concluded as more accurate due to a more detailed model. There can be several different reasons behind this, one being that the battery thermal model is inaccurate, generating more heat when driving than expected. As a result of the heat exchange model between the battery pack and ambient temperature being simplified, the transfer of heat is not dependent on the velocity and acceleration of the vehicle. Consequently, less heat is dissipated from the battery pack at higher velocities and accelerations could explain the observed higher temperature levels. Another factor that may contribute to this is the amount of heat transferred to the battery pack from the electric powertrain. The intricacy of the TMS within the powertrain resulted in a simplified modeling approach, hence modeled as 3% of the total energy consumed due to propulsion. However, in reality, this system is systematically managed to optimize the temperature of critical components and the deviations of the result indicate that the assumption made was not accurate.

At certain charging stops along the route, the temperature exceeds what is referred to as optimal. This can be contributed to that the model lacks a comprehensive onboard cooling system consisting of heat exchangers and pumps. As a result of this, the model is not always able to regulate the temperature to the desired optimal level before reaching a charger. To combat this the optimal charging temperature could be integrated into the algorithm and be a part of the decision-making of choosing a charger.

5.1.3 Limited data for charging models

Section 3.3.1 highlighted the limitations of the data collected for the charging models, specifically in terms of a limited number of tests and parameters. To develop a more accurate model, a substantial amount of data from various scenarios for the specified vehicle is needed. Additionally, minimizing differences between tests is crucial to minimize errors. This could not be regulated, resulting in varying preconditions for each test.

Due to the lack of data, assumptions had to be made. These assumptions include the charging power of the charger, starting temperature of the battery, contributing factors to energy loss, and the proportional relationship between the TTC and the battery's capacity. Despite these challenges, the approach of gathering as much data as possible and fitting a regression model to filter out differences yielded great results. Nevertheless, it is important to acknowledge the limitations formed by the constrained data collection process and the assumptions that came with it.

5.1.4 Conclusion of the optimization algorithm

In Section 4.5 the optimization algorithm identified that route 3 was the most optimal of the three possible, both in regards to time and distance as seen in Table 4.4. This together with the verification against other services such as ABRP, where the algorithm gives similar results in the selection of route, Figure 4.12, confirms the belief that the selected route is the optimal one. The chosen charging stations are hard to verify if they are optimally chosen, but the result on all three routes seems reasonable on the given values, that all chosen chargers have an SoC value lower than 40 %. The distances are evenly spread out as seen in Figures 4.9, 4.2 and 4.3, and Table 4.5. In the table, the charging time can seem to be similar to those from ABRP, which is a confirmation that the difference is primarily in energy consumption.

The current state of the algorithm could benefit from greater utilization of the stochastic model. However, as mentioned in Section 4.2, the lack of sufficient data limits its correlation with reality. If a larger data set had been collected during the data collection phase, the transition matrices could have incorporated temporal dependencies, and the initial state distribution vector could have been based on data from a specific time period. This would have made the cost calculated from the stochastic model more influential in charger selection, giving it greater weight.

The algorithm is optimized for the current road in one direction. If the project was to be expanded upon in choice of travel route, another implementation of the route planning algorithm would have to be constructed with the ability to move between roads more freely.

In conclusion, the project has successfully accomplished its goal of serving as a proof of concept for combining stochastic models for charger availability, mathematical modeling of vehicle dynamics, and optimizing the charging and temperature control

into an algorithm that can determine an optimal route for a BEV. This is evident from the result given in Section 4.5.

5.2 Future works

Going forward, modeling and evaluating a more intricate TMS would greatly benefit the algorithm, and produce a more accurate simulation of the battery temperature. Also integrating the battery temperature in the decision-making of choosing chargers would assure that the optimal temperature of charging always is upheld. As well as including a complete model of the auxiliary loads to decrease the degree of error in the longitudinal vehicle dynamics model. An improvement to the predetermined routes would be to, instead of collecting singular points on the road, construct a road grid similar to Google Maps, that could contain all information on the routes, including, speed limits, elevation, etc. This would prevent the algorithm from iterating discreetly through the points on the road and allows for a more continuous and dynamic updating implementation.

Additionally, more reliable data collection is needed to ensure accuracy in the models, either via an agreement with Chargefinder or the use of another data source. With more charging station data, a time-dependent charger availability model could be implemented.

Bibliography

[1] H. Ritchie. *Sector by sector: where do global greenhouse gas emissions come from?*. Our World in data; 2020 [Cited 2023 April 28]. Available from: https://ourworldindata.org/ghg-emissions-by-sector

[2] C. Buysse, J. Miller. *Transport could burn up the EU's entire carbon budget.* The international council of clean transport; 2021.[Cited 2023 April 28] Available from: https://theicct.org/transport-could-burn-up-the-eus-entire-carbon-budget/

[3] Europaparlamentet. *EU:s förbud mot försäljning av nya bensin- och dieselbilar från 2035 förklarat* Europaralamentet; 2023. [Cited 2023 April 28] Available from: https://www.europarl.europa.eu/news/sv/headlines/economy/20221019STO44572/eu-s-forbud-mot-forsaljning-av-nya-bensin-och-dieselbilar

[4] Transport & environment. *Electric cars emit less CO2 over their lifetime than diesels even when powered with dirtiest electricity – study* Transport & environment; 2017. [Cited 2023 April 29]
Available from: https://www.transportenvironment.org/discover/electric-cars-emit-less-co2-over-their-lifetime-diesels-even-when-powered-dirtiest-electricity/

[5] IEA. *Global EV Outlook 2021* IEA; 2021. [Cited 2023 April 29] Available from: https://www.iea.org/reports/global-ev-outlook-2021

[6] . M. Carlier. *Automotive industry worldwide - statistics & facts* Statista; 2023. [Cited 2023 April 29] Available from: https://www.statista.com/topics/1487/automotive-industry/#topicOverview

[7] Z. Bastin, S. Bhattacharya, A. Kumar. *INTERNATIONAL ELECTRIC-VEHICLE CONSUMER SURVEY.* Alixpartners; 2019. [Cited 2023 April 29] Available from: //www.alixpartners.com/media/13453/ap-electric-vehicle-consumer-study-2019.pdf

[8] (2020) G. Henrique Ruffo. *How Much Does The Powertrain Represent Out Of Total Cost For An EV?* Insideeves; 2020 [Cited 2023 April 30]. Available from: https://insideevs.com/features/396979/how-much-powertrain-cost-ev/

[9] Regeringskansliet *I en värld som ställer om - Sverige utan fossila drivmedel 2040* Regerinskansliet; 2021 [Cited 2023 April 30]. Available from: https://www.regeringen.se/rattsliga-dokument/statens-offentliga-utredningar/2021/06/sou-202148/

[10] European Commission *European Alternative Fuels Observatory: Sweden* European Comission; 2022 [Cited 2023 April 30]. Available from: https://alternative-fuels-observatory.ec.europa.eu/transport-mode/road/sweden

[11] Recurrent. *Winter Cold Weather EV Range Loss in 7,000 Cars.* [Internet]. Recurrent; 2022. [Cited 2023 April 10]. Available from: https://www.recurrentauto.com/research/winter-ev-range-loss

[12] C.Argue. *To what degree does temperature impact EV range?.* [Internet]. GEOTAB; 2023. [Cited 2023 April 11]. Available from: https://www.geotab.com/blog/ev-range/

[13] World economic forum. *Electric vehicles: The 3 main factors holding back sales.* [Internet]. World economic forum; 2022. [Cited 2023 April 11]. Available from: https://www.weforum.org/agenda/2022/10/ev-sales-charging-infrastructure-transport-sector-sustainable

[14] E.Figenbaum, S. Nordbakke. *Battery electric vehicle user experiences in Norway's maturing market.* [Internet]. Norway: Institue of transport economics Norwegian center for transport research; 2019. [Cited 2023 April 11]. Available from: https://www.toi.no/publications/battery-electric-vehicle-user-experiences-in-norway-s-maturing-market-article35709-29.html

[15] E.Figenbaum. *Electromobility Status in Norway: Mastering Long Distances – the Last Hurdle to Mass Adoption.* [Internet]. Norway: Institute of Transport Economics; 2018. [Cited 2023 April 9]. Available from: https://trid.trb.org/view/1509475

[16] G.Batra, A.Khatri, A.Goel and M.Samant. *EY Mobility Consumer Index 2022 study.* [Internet]. EY; 2022. [Cited 2023 April 23]. Available from: https://assets.ey.com/content/dam/ey-sites/ey-com/en_gl/topics/automotive-and-transportation/automotive-transportation-pdfs/ey-mobility-consumer-index-2022-study.pdf

[17] S.Harryson, M.Ulmefors, A.Kazlova *Overview and analysis of electric vehicle incentives applied across eight selected country markets.* [Internet]. Blekinge: Blekinge tekniska universitet; 2015. [Cited 2023 April 4]. Available from: https://www.diva-portal.org/smash/get/diva2:882227/FULLTEXT01.pdf

[18] S.Harshit. *Why do the majority of EVs get a single-speed gearbox and not a multi-speed gearbox?* Evoindia; 2021 [Cited 2023 April 10]. Available from: https://www.evoindia.com/features/difference-between-single-speed-gearbox-and-multi-speed-gearbox-in-evs-explained

[19] Battery design *Open Circuit Voltage* Batterydesign; 2016 [Cited 2023 March 25]. Available from: https://www.batterydesign.net/electrical/open-circuit-voltage/

[20] Battery design *Specific Heat Capacity of Lithium Ion Cells* Batterydesign; 2022. [Cited 2023 April 10]. Available from: https://www.batterydesign.net/specific-heat-capacity-of-lithium-ion-cells/

[21] A.Hamednia, et al. *Optimal Thermal Management, Charging, and Eco-driving of Battery Electric Vehicles* [Internet]. Gothenburg: Chalmers university of technology; 2020 [Cited 2023 March 2]. Available from: https://arxiv.org/pdf/2205.01560.pdf

[22] K. Liang, et al. *Data-Driven Ohmic Resistance Estimation of Battery Packs for Electric Vehicles* [Internet]. Beijing: Beijing Institute of Technology; 2019 [Cited 2023 April 15] Available from: https://doi.org/10.3390/en12244772

[23] A. Nuhic, et al. *Health diagnosis and remaining useful life prognostics of lithium-ion batteries using data-driven methods* [Internet]. J Power Sources: 2013. [Cited 2023 April 15] Available from: https://doi.org/10.1016/j.jpowsour.2012.11.146

[24] F. Bülow T.Meisen. *A review on methods for state of health forecasting of lithium-ion batteries applicable in real-world operational conditions.* [Internet. Journal of Energy Storage; 2023. [Cited 2023 April 15] Available from: https://doi.org/10.1016/j.est.2022.105978

[25] Hyundai Motor Group *EV A to Z Encyclopedia - 1: Understanding EV Components.*[Internet]. Hyundai Motor Group; 2020. [Cited 2023 April 15]. Available from: https://www.hyundaimotorgroup.com/story/CONT0000000000000906

[26] O.Juhlin. *Modeling of Battery Degradation in Electrified Vehicles.* [Internet]. Linköping: Linköping University; 2016. [Cited 2023 April 15]. Available from: https://liu.diva-portal.org/smash/get/diva2:1067565/FULLTEXT01.pdf

[27] National Grid *What happens to old electric car batteries?.* [Internet]. National Grid; 2022. [Cited 2023 April 16]. Available from: https://www.nationalgrid.com/stories/journey-to-net-zero-stories/what-happens-old-electric-car-batteries

[28] Northvolt. *Europe's largest electric vehicle battery recycling plant begins operations.* [Internet]. Northvolt; [cited 2023 May 16]. Available from: https://northvolt.com/articles/hydrovolt/

[29] J.Lowry, J.Larminie *Electric Vehicle Technology Explained*, 2nd Edition [Internet]. 2nd ed. Wiley; 2012 [cited 2023 May 14]. Available from: https://www.wiley.com/en-us/Electric+Vehicle+Technology+Explained%2C+2nd+Edition-p-9781119942733

[30] J.Choksey. *What is Regenerative Braking?* [Internet]. J.D. Power; 2021. [cited 2023 April 16]. Available from: https://www.jdpower.com/cars/shopping-guides/what-is-regenerative-brakin

[31] Reimpell J, Stoll H, Betzler J. *The Automotive Chassis: Engineering Principles.* 2nd ed. [Internet]. Burlington, MA: Butterworth-Heinemann; 2001.[Cited 2023 April 17]. Available from: https://doi.org/10.1016/B978-0-7506-5054-0.X5000-7

[32] Wargula Ł, Wieczorek B, Kukla M. *The determination of the rolling resistance coefficient of objects equipped with the wheels and suspension system – results of preliminary tests.* MATEC Web of Conferences [Internet]. 2019 [cited 2023 April 17]. Available from: https://doi.org/10.1051/matecconf/201925401005

[33] LibreTexts. *Drag Force and Terminal Speed. In: University Physics I - Mechanics, Sound, Oscillations and Waves.*[Internet]. LibreTexts; 2016. [Cited 2023 April 16]. Available from: https://phys.libretexts.org/Bookshelves/University_Physics.

[34] Polestar. *PRESS KIT – POLESTAR 2.*[Internet]. Polestar; 2022. Available from: https://www.polestar.com/bynder-assets/m/3b46df57d0e5580c

[35] Björnsson LH, Karlsson S. *The potential for brake energy regeneration under Swedish conditions.* [Internet]. Applied Energy; 2016. [Cited 2023 April 19]. Available from: https://doi.org/10.1016/j.apenergy.2016.01.051

[36] B.Gao , Y.Yan, H.Chu, H.Chen, N.Xu. *Torque allocation of four-wheel drive EVs considering tire slip energy* [Internet]. Science China Information Sciences; 2021. [Cited 2023 April 19]. Available from: https://link.springer.com/article/10.1007/s11432-019-2946-8

[37] Incropera FP, DeWitt DP, Bergman TL. *Incropera's Principles of Heat and Mass Transfer.* 7th ed. Hoboken, NJ: John Wiley & Sons, Inc.; 2019 [Cited 2023 April 23].

[38] J.Nayar. *Not-So-Green Technology: The Complicated Legacy of Rare Earth Mining.* [Internet]. Harvard International Review; 2021 [cited 2022 May 4];. Available from: https://hir.harvard.edu/not-so-green-technology-the-complicated-legacy-of-rare-earth-mining/

[39] Tesla. (n.d.). *Our supply chain.* Tesla; 2023. [Cited 2023 April 23]. Available from: https://www.tesla.com/impact/supply-chain

[40] Impact. *Electric vehicle battery modules and packs* [Internet]. Interplex; [cited 2022 May 4]. Available from: https://interplex.com/electric-vehicle-battery-modules-and-packs/

[41] CFD Flow Engineering. *Battery Cooling Techniques in Electric Vehicle.* [Internet]. [Cited 2023 May 11]. Available from: https://cfdflowengineering.com/battery-cooling-techniques-in-electric-vehicle/#Liquid_cooling_of_Battery.

[42] LI J, ZHU Z. *Battery Thermal Management Systems of Electric Vehicles.* [Internet]. Master's Thesis in Automotive Engineering. Department of Applied Mechanics, Division of Vehicle Engineering & Autonomous Systems, Road Vehicle Aerodynamics and Thermal Management, Chalmers University of Technology, Göteborg, Sweden; 2014. [Cited 2023 April 14]. Available from: https://publications.lib.chalmers.se/records/fulltext/200046/200046.pdf

[43] Luo J, Zou D, Wang Y, Wang S, Huang L *Battery thermal management systems (BTMs) based on phase change material (PCM): A comprehensive review* [Internet] Chemical Engineering Journal; 2021. [Cited 2023 April 23]. Available from: https://doi.org/10.1016/j.cej.2021.132741

[44] Laddboxbolaget. *Skillnaden mellan AC-laddning och DC-laddning* [Internet]. Sweden: Laddboxbolaget; 2022 [Cited 2023 April 14]. Available from: https://laddboxbolaget.se/skillnaden-mellan-ac-laddning-och-dc-laddning/

[45] OKQ8 *Hur mycket kostar det att ladda en elbil?* [Internet]. Sweden: OKQ8; 2022 [Cited 2023 April 14]. Available from: https://www.okq8.se/medlem/artiklar/hur-mycket-kostar-det-att-ladda-en-elbil/

[46] B.Nyland. *B.Nyland public charger and BEV test results.* [Internet]. Norway: B.Nyland; 2020. [Cited 2023 May 10]. Available from: https://shorturl.at/uxOU3

[47] Accelerationtimes.com *Volvo XC40 P8 Recharge acceleration times in kilometers per hour* [Internet]. Accelerationtimes.com; 2022 [Cited 2023 April 4]. Available from: https://accelerationtimes.com/models/volvo-xc40-p8-recharge

[48] Trafikverket *NVDB* [Internet]. Sweden: Trafikverket; 2023. [Cited 2023 April 4]. Available from: https://nvdb2012.trafikverket.se/

[49] Volvo Cars. *XC40 Recharge Pure Electric - Tekniska specifikationer*. [Internet]. Göteborg: Volvo Car Corporation; 2021 [cited 2022 May 16]. Available from: https://www.volvocars.com/se/cars/xc40-electric/specification/.

[50] M.Fojtlína, M.Planka, J.Fišer, J.Pokorný, M.Jíchal *Airflow Measurement of the Car HVAC Unit Using Hot-wire Anemometry* [Internet]., Czech Republic: Brno University of Technology; 2016. [Cited 2023 April 5]. Available from: https://doi.org/10.1051/epjconf/201611402023

[51] UL research institute *What Causes Thermal Runaway?* [Internet]. UL research institute; 2021. [Cited 2023 April 5]. Available from: https://shorturl.at/ACS05

[52] C.Un, K.Aydın. *Thermal Runaway and Fire Suppression Applications for Different Types of Lithium Ion Batteries.* [Internet]. Turkey: Çukurova University; 2021. [Cited 2023 April 5]. Available from: https://doi.org/10.3390/vehicles3030029

[53] D.Kroese, R.Rubinstein. *Monte Carlo methods* [Internet]. Wires computational statistics; 2011. [Cited 2023 May 9]. Available from: https://doi.org/10.1002/wics.194

[54] P.Sokorai, A.Fleischhacker, G.Lettner, H.Auer. *Stochastic Modeling of the Charging Behavior of Electromobility.* . World Electric Vehicle Journal [Internet]. 2018 Oct 22;9(3):44. Available from: http://dx.doi.org/10.3390/wevj9030044

A

Appendix 1

A.1 Charger data collection code

```
headers = {
    'pragma': 'no-cache',
    'cache-control': 'no-cache',
    'sec-ch-ua': '" Not;A Brand";v="99", "Google Chrome";v="91", "
   Chromium";v="91"',
    'accept': 'application/json, text/plain, */*',
    'sec-ch-ua-mobile': '?0',
    'applicationversion': '331.0.2',
    'user-agent': 'Mozilla/5.0 (X11; Ubuntu; Linux x86_64; rv:89.0)
    Gecko/20100101 Firefox/89.0',
    'sec-fetch-site': 'same-origin',
    'sec-fetch-mode': 'cors',
    'sec-fetch-dest': 'empty',
    'accept-language': 'en-US,en;q=0.9',
}
```

Listing A.1: API request headers

```
f = open("outletListDict.txt", "a")

for n, charger in enumerate(chargers_id):
    print("Organizing " + charger + " " + (str(n) + "/" + str(len(
   chargers_id))))

    station_res = requests.get('https://api.chargefinder.com/
   station/' + charger, headers=headers)
    status_res = requests.get('https://api.chargefinder.com/status/
   ' + charger, headers=headers)

    id_to_index = []

    index = 0
    for outletList in station_res.json()['outletList']:
        for outlet in outletList['outlets']:
            id_to_index.append([index, outlet['identifier'], outlet
   ['name']])
        index += 1

    for c in status_res.json():
```

```
        c_id = c['id']
        for id_or_name in id_to_index:
            if id_or_name[2] == c_id or id_or_name[1] == c_id:
                if(charger + c_id in outletListDict):
                    print("ERROR! Duplicate ID: " + c_id)
                outletListDict[charger + c_id] = id_or_name[0]
                f.write(charger + c_id + " " + str(id_or_name[0]) +
    "\n")
                break

f.close()
```

Listing A.2: Generating dictionary of outlets to group index

```
if res.status_code != 200:
        if res.status_code != 403:
            print("Error: " + str(res.status_code) + " (continuing
    ...)")
            return []

        forbidden_c = 0
        while(res.status_code == 403):
            forbidden_c += 1
            if forbidden_c > 3:
                print("Too many 403 errors, skipping...")
                return []
            print("403 error, waiting 2 minutes...")
            time.sleep(120)
            res = requests.get('https://api.chargefinder.com/status
    /' + id, headers=headers)
```

Listing A.3: Error handling on logger

A.2 Battery temperature over time at ambient temperature 0°C for route 1-3

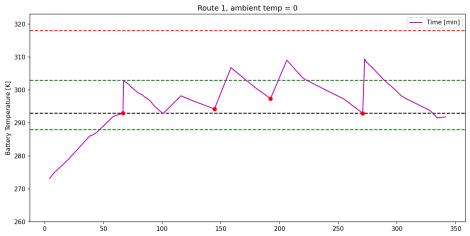

Figure A.1: Battery temperature over time at ambient temperature 0°C for route 1

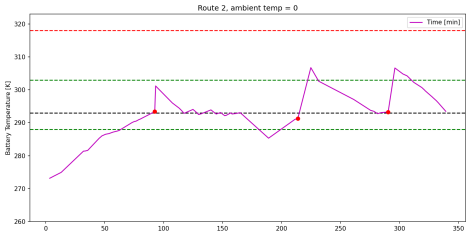

Figure A.2: Battery temperature over time at ambient temperature 0°C for route 2

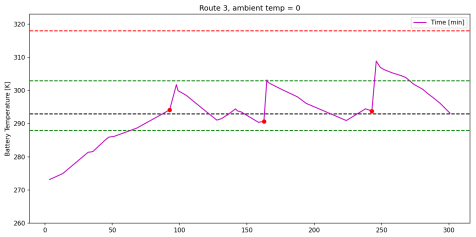

Figure A.3: Battery temperature over time at ambient temperature 0°C for route 3

A.3 Battery temperature over distance at ambient temperature 0°C for route 1-2

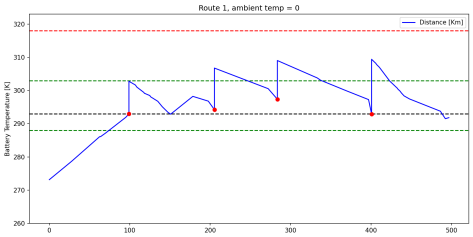

Figure A.4: Battery temperature over distance at ambient temperature 0°C for route 1

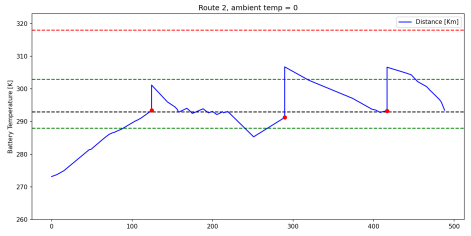

Figure A.5: Battery temperature over distance at ambient temperature 0°C for route 2.

A.4 Energy consumption over distance at ambient temperature 0°C for route 1-2

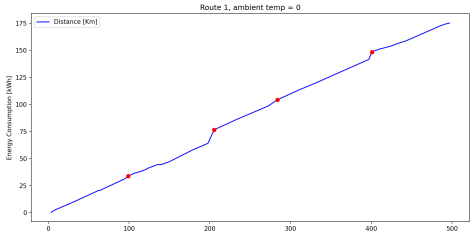

Figure A.6: Energy consumption over distance at ambient temperature 0°C for route 1.

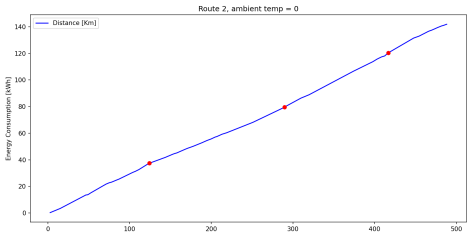

Figure A.7: Energy consumption over distance at ambient temperature 0°C for route 2.

A.5 Energy consumption over time at ambient temperature 0°C for route 1-3

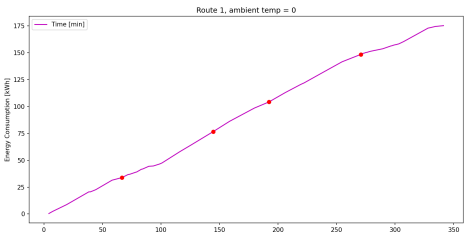

Figure A.8: Energy consumption over time at ambient temperature 0°C for route 1.

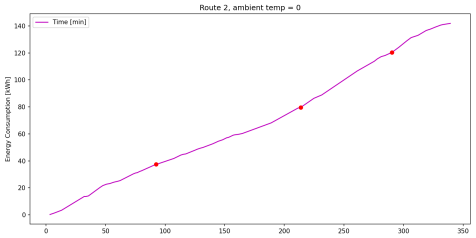

Figure A.9: Energy consumption over time at ambient temperature 0°C for route 2.

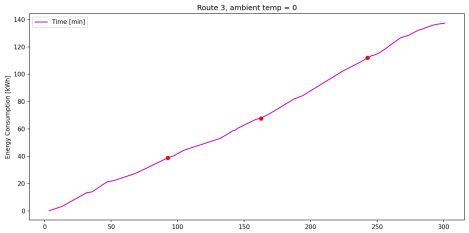

Figure A.10: Energy consumption over time at ambient temperature 0°C for route 3.

A.6 SoC over distance at ambient temperature 0°C for route 1-2

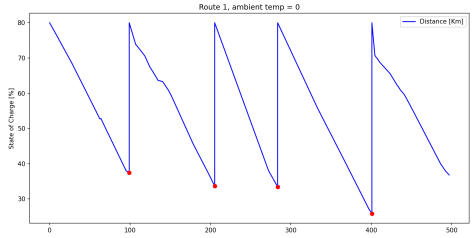

Figure A.11: SoC over distance at ambient temperature 0°C for route 1

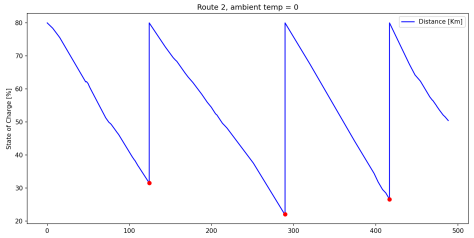

Figure A.12: SoC over distance at ambient temperature 0°C for route 2.

A.7 SoC over time at ambient temperature 0°C for route 1-3

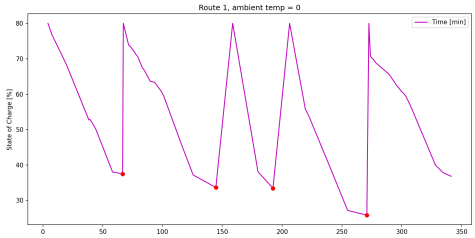

Figure A.13: SoC over time at ambient temperature 0°C for route 1

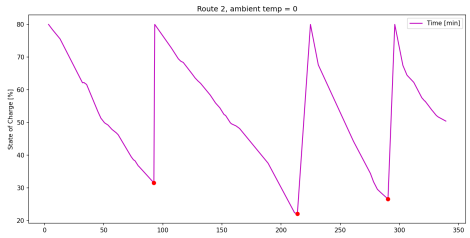

Figure A.14: SoC over time at ambient temperature 0°C for route 2.

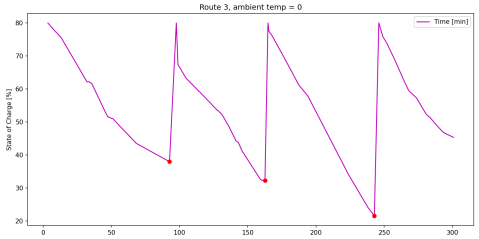

Figure A.15: SoC over time at ambient temperature 0°C for route 3.

A.8 Algorithm code from GitHub

Link to the complete algorithm code: https://github.com/snikaren/Kandidatarbete?fbclid=IwAR0iBX5UI5YG2FERxOraTl1Q4ldfLu2AyAbF1aDqyBfHcGHuA3NvbeCrFMo

DEPARTMENT OF ELECTRICAL ENGINEERING
CHALMERS UNIVERSITY OF TECHNOLOGY
Gothenburg, Sweden
www.chalmers.se

CHALMERS